Upward range shift of a dominant alpine shrub related to 50 years of snow cover change

Reference:
Zong Shengwei, Lembrechts Jonas, Du Haibo, He Hong S., Wu Zhengfang, Li Maihe, Rixen Christian.- Upward range shift of a dominant alpine shrub related to 50 years of snow cover change
Remote sensing of environment - ISSN 1879-0704 - 268(2022), 112773
Full text (Publisher's DOI): https://doi.org/10.1016/J.RSE.2021.112773
To cite this reference: https://hdl.handle.net/10067/1833230151162165141

Upward range shift of a dominant alpine shrub related to 50 years of snow cover change

Shengwei Zong[a], Jonas J. Lembrechts[b], Haibo Du[a], Hong S He[*,c,a], Zhengfang Wu[*,a], Maihe Li[d], Christian Rixen[e]

[a] Key Laboratory of Geographical Processes and Ecological Security in Changbai Mountains, Ministry of Education, School of Geographical Sciences, Northeast Normal University, 130024 Changchun, China

[b] Research Center Plants and Ecosystems, University of Antwerp, 2610 Wilrijk, Belgium

[c] School of Natural Resources, University of Missouri, 65211 Columbia, MO, USA

[d] Swiss Federal Institute for Forest, Snow and Landscape Research WSL, CH-8903 Birmensdorf, Switzerland

[e] WSL Institute for Snow and Avalanche Research SLF, 7260 Davos Dorf, Switzerland

* Corresponding author

E-mail address of each author

Shengwei Zong: zongsw049@nenu.edu.cn

Jonas J. Lembrechts: lembrechtsjonas@gmail.com

Haibo Du: duhb655@nenu.edu.cn

Hong S He: heh@missouri.edu

Zhengfang Wu: wuzf@nenu.edu.cn

Maihe Li: maihe.li@wsl.ch

Christian Rixen: rixen@slf.ch

Abstract

Pronounced climate warming has resulted in a significant reduction of snow cover extent, as well as poleward and upslope shifts of shrubs in Arctic and alpine ecosystems. However, it is difficult to establish links between changes in snow cover and shrub distribution changes due to a lack of *in situ* and long-term snow records in relation to abundance shifts of shrubs at their leading (i.e., cold) and trailing (i.e., warm) edges. We used remote sensing to extract long-term changes in both snow cover and shrub distributions in response to climate change in the alpine tundra of the Changbai Mountains in Northeast China. First, we analyzed spatio-temporal changes in snow cover during the snowmelt period (April 1st to June 15th) over the past 54 years (1965–2019). Then, we analyzed distribution changes of the dominant evergreen alpine shrub, *Rhododendron aureum*, using 31 years (1988–2019) of Landsat NDVI archives. We applied a novel approach by analyzing NDVI data from autumn only, when *R. aureum* is green yet most of the surrounding plants are already brown. Finally, we tested the relationship between snowmelt date and the distribution of *R. aureum*. We found that the fraction cover of *R. aureum* experienced greater loss than gain in the last 30 years. *R. aureum* expanded at the leading edge, establishing in snow-rich habitats, yet retracted further at the trailing edge due to loss of snow habitats. We identified the preferred snowmelt regime (habitats with snowmelt date of 20 April or later) of this shrub species and found that further advances in snowmelt dates would lead to the upward range shift of *R. aureum* in a warming climate. Our results indicate that spring snow cover change affected distribution changes of *R. aureum*. Our study highlights that long-term changes in snow cover due to climate change have already had marked impacts on plant species distributions in alpine ecosystems.

Keywords: Snow cover change; Evergreen shrub; Distribution change; Species distribution modelling

Highlights

The fraction cover of *R. aureum* in the Changbai Mountains experienced greater loss than gain in the last 30 years.

Changes in leading and trailing edges of *R. aureum* related to snow cover trends in the last 50 years.

Further advance in snowmelt dates would lead to the upward range shift of *R. aureum*.

1. Introduction

Snow is an important component of cold biomes, controlling local-scale environmental conditions (e.g., soil temperature and moisture), defining growing season length, and determining plant distribution patterns (Billings and Bliss, 1959; Keller et al., 2005; Walker et al., 2001; Wipf et al., 2009). During the past decades, pronounced climate warming in Arctic and alpine ecosystems has resulted in a significant reduction of snow cover extent (Bokhorst et al., 2016; Klein et al., 2016; Marty et al., 2017). Meanwhile, shrub species, which are often the characteristic and dominant species in cold biomes, have been observed to shift poleward and upslope in geographic distribution (Formica et al., 2014; Malfasi and Cannone, 2020; Martin et al., 2017; Myers-Smith et al., 2015; Scharnagl et al., 2019; Tape et al., 2006). Snow cover change has been found to affect shrub phenology, growth, and abundance via indirect effects on soil conditions and frost exposure (Cooper et al., 2019; Daniëls et al., 2015; Francon et al., 2020; Gerdol et al., 2013; Matteodo et al., 2016; Sturm et al., 2001; Wheeler et al., 2014; Wipf and Rixen, 2010). However, it is difficult to establish links between changes in snow cover and in shrub distribution because there is a lack of *in situ* and long-term snow records in relation to abundance shifts of shrubs at their leading (i.e., cold) and trailing (i.e., warm) edges (Hallinger et al., 2010). This knowledge gap prevents an in-depth understanding of future plant distribution changes in cold biomes in the context of climate warming.

Remote sensing is a practical way to obtain snow cover information (Hall, 2012). Several studies have indicated that understanding snow data derived from remote sensing are beneficial for understanding plant distribution changes in cold biomes (Beck et al., 2005; Carlson et al., 2015; Niittynen and Luoto, 2018; Randin et al., 2009). Nevertheless, long-term snow cover products for recent decades of accelerated climate change are still rare, especially for alpine regions where snow cover changes occur at fine scales in rugged terrain (Carlson et al., 2013; Dedieu et al., 2016). Snow cover information can be extracted from optical satellite imagery, such as the Landsat series, the longest available record among the different satellite observation platforms. However, determining snow cover extent faces a number of methodological issues. Changeable weather in mountainous regions and long return intervals of optical satellites can make it difficult to obtain continuous cloud-free observations (Rosenthal and Dozier, 1996). Furthermore, redistribution of snow occurs frequently because of changing wind drift, snow avalanches, and multiple snowfalls in winter (Hiemstra et al., 2002), which increases the difficulty of capturing the ever-changing snow distribution to derive accurate snow cover duration. However, a useful period to define snow cover change is during the spring snowmelt season, which is widely believed to be a critical period for plant growth and distribution (Cooper et al., 2011; Heegaard, 2002; Keller et al., 2005; Wipf, 2010). During this period, the snowmelt pattern regulates several abiotic constraints, such as the number and intensity of spring freezing events. Thus it acts as a filter determining community composition and plant distributions (Good et al., 2019; Winkler et al., 2018). Sensitive responses of shrubs (phenology, growth, and regeneration) to snowmelt date have been demonstrated in experimental and observational studies (Carbognani et al., 2014;

Francon et al., 2020; Klanderud and Birks, 2003; Mallik et al., 2011; Rixen et al., 2010; Sandvik and Odland, 2014; Wheeler et al., 2014), indicating that shrub distribution change is closely related to snow cover during the snowmelt season.

Shrub distribution changes in cold biomes have been assessed based on long-term plot monitoring and analysis of repeated field photos (Formica et al., 2014; Myers-Smith et al., 2015; Tape et al., 2006), but the detection of large-scale changes in shrub cover has been hampered by a lack of historical records with sufficient scale or resolution (Beamish et al., 2020; van Lier et al., 2009). Therefore, remote sensing has a high potential to capture entire shrub distribution ranges, though it is still a significant challenge to detect shrub cover in Arctic and alpine vegetation due to heterogeneous species composition and ground cover (Bayle et al., 2019; Räsänen and Virtanen, 2019). However, arctic and alpine shrubs, e.g., from the Ericaceae family, often form single-species dominant clusters that can cover areas that are large enough to detect with high-resolution imagery (e.g., aerial photos). High-resolution imagery is, however, not available for extracting historical shrub distribution in many cold regions, again due to lack of historical coverage (Greaves et al., 2016). Pixel-level analyses of trends in vegetation greening (i.e., assessing trends in time series of spectral vegetation indices derived from optical satellite imagery) have been related to the observed shrub expansion and encroachment in Arctic and alpine ecosystems (Berner et al., 2020; Carlson et al., 2017; Forbes et al., 2010; Macias-Fauria et al., 2012). However, processes at both leading and trailing edges are often difficult to detect, especially at the species level. In most studies, precisely relating an increase in shrub occurrence to greening signals – using the maximum values of spectral vegetation indices (e.g., normalized difference vegetation index, NDVI) – has proven difficult because several plant communities exhibit similarly high greenness values at the peak of the growing season (Myers-Smith et al., 2020). A possible solution to differentiate between species is to analyze greenness in different seasons. So far, this use of key phenological anomalies has rarely been tested in Arctic and alpine vegetation studies but has been used in remote sensing studies concerning the mapping of invasive plants (Bradley, 2014; Labonté et al., 2020; Peterson, 2005; Weisberg et al., 2017). A useful but neglected period to identify and track shrubs is autumn, when the phenological trajectories of many plants diverge from one another (Bayle et al., 2019; Filippa et al., 2019). Due to a high chlorophyll or anthocyanin content of leaf tissue in autumn, both deciduous ericaceous shrubs (e.g., *Vaccinium uliginosum*) with red leaves and evergreen ericaceous shrubs (e.g., *Rhododendron ferrugineum*) with green leaves have been observed to exhibit distinctive green or red reflectance values compared with those of sedges and grasses with brown leaves (Bayle et al., 2019; Hughes, 2011). Such phenological differences in autumn provide a promising solution for mapping and tracking shrubs over time.

In this study, we aimed to identify long-term spring snow dynamics and to extract distribution changes of an alpine dominant and evergreen ericaceous shrub, *Rhododendron aureum*, which grows in habitats with sufficient snow cover in the alpine tundra of the Changbai Mountains, Northeast China. We obtained the distribution of *R. aureum* by means of autumn greenness values and linked this information to data on snow melting date (and changes therein), using a range of remote sensing products and transect plots for ground truthing. We hypothesized that: (i) spring snow cover extent decreased over the last 50 years due to climate warming, indicating a shrinking cryosphere in alpine ecosystems; (ii) during the last 30 years, *R. aureum* decreased in cover at the trailing (lower-elevation) edge of its distribution and increased at the leading (higher-elevation) edge; and (iii) a loss of snow habitats was a main environmental driver for the upward elevational shift in *R. aureum* cover.

2. Materials and Methods

2.1 Study area

The Changbai Mountains are located in Northeast China (41°41′49″ to 42°25′18″N and 127°42′55″ to 128°16′48″E) at the border with North Korea (Figure 1). Tree line position in the region is generally below 1850 m, and the alpine tundra extends from 1850 to the mountain summit at 2749 m. Annual mean temperature is -6.67 °C, and annual average precipitation is 958 mm at the mountain summit (Zong et al., 2016). The dominant rock substrate is of volcanic origin, such as breccia, pumice and volcanic ash. Spring is from April to June and growing season of tundra vegetation usually starts from May and ends in early September. The spring snowmelt period lasts from ca. April to June in the alpine tundra. Snow cover can persist in gullies and shady slopes for about one month longer than at adjacent exposed sites.

The alpine tundra located at the top of the Changbai volcano has been without human disturbance (e.g., grazing) for several hundred years. The latest major volcanic eruption in the Changbai Mountains occurred in 1702, destroying all alpine tundra vegetation (Liu et al., 1998). The present alpine tundra vegetation has thus recolonized the area over the last three hundred years. The vegetation succession is still on-going as mountain birch forests were observed moving upward (Zong et al., 2014). Dominant plant species include the evergreen shrub *Rhododendron aureum*, as well as deciduous dwarf shrubs like *Vaccinium uliginosum* and *Dryas octopetala* var. *asiatica* (Wada and Nakai, 2004), sedge communities dominated by *Carex pseudo-longerostrata*. Especially at lower elevations, communities with herbaceous plants such as grasses (e.g., *Deyeuxia* spp.*)* are abundant.

Known as a representative and dominant alpine tundra species across Northeast Asia (Kudo, 1993), *R. aureum* is the only evergreen plant species that frequently forms single-species clusters in this study area. *R. aureum* is not a typical alpine species that tolerates frost. It requires snow cover protection from extreme low temperatures to survive in the alpine ecosystem (Liu et al., 2009; Zhang et al., 2010). Climate warming has significantly advanced spring snowmelt date and shortened snow cover duration, which in turn has affected the survival and distribution of *R. aureum*. This phenomenon has also been observed in other regions of Northeast Asia (Kudo, 1991; Kudo, 1993; Kudo and Ito 1992). In addition, *R. aureum* benefits from snow environments because snow prevents frost damage and provides sufficient water for growth during the spring snowmelt season (Liu et al., 2009; Zhang et al., 2010). This habitat preference of *R. aureum* allowed us to link spring snow cover change to

R. aureum distribution changes.

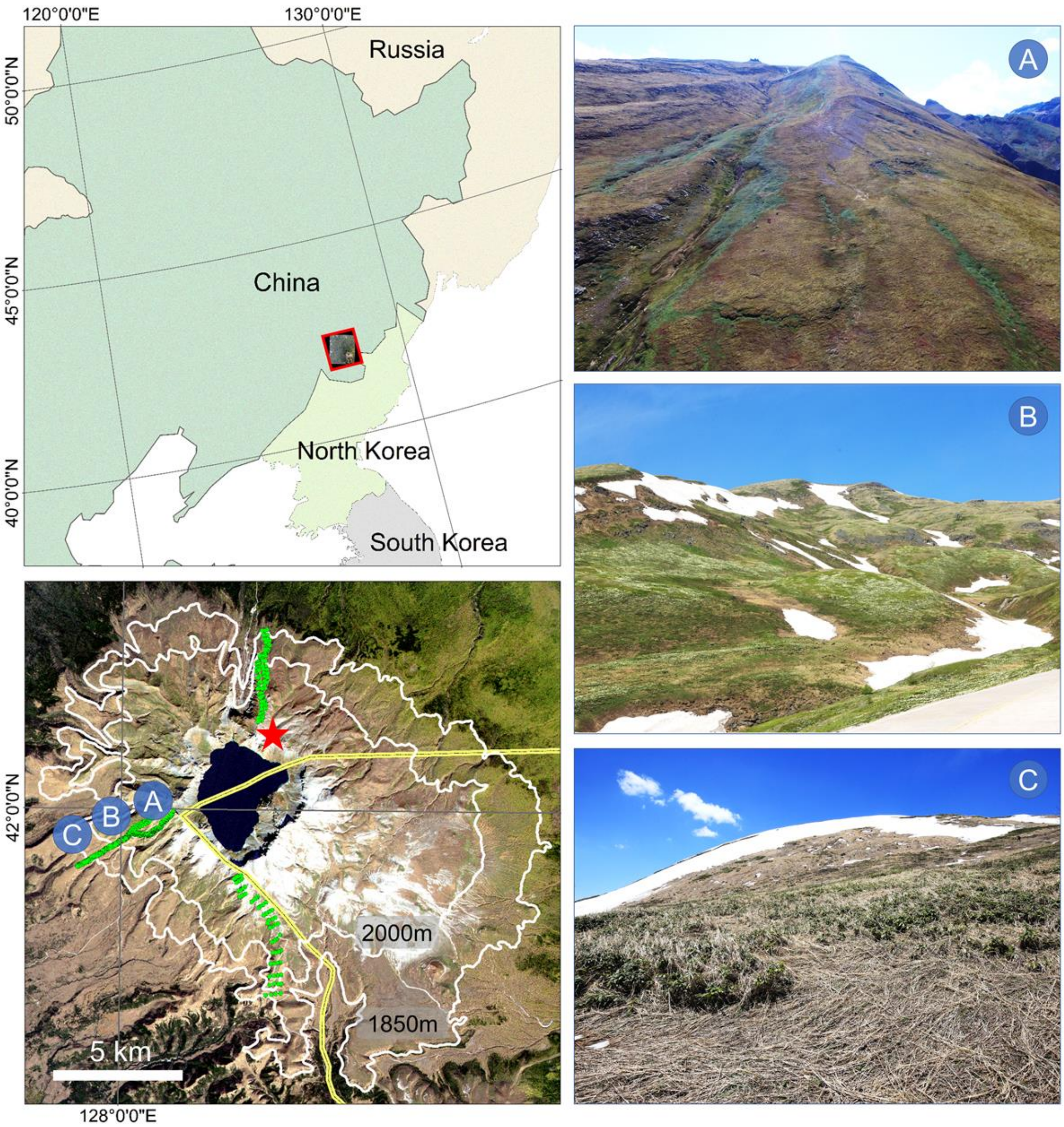

Figure 1. Upper Left: location of Changbai Mountains in Northeast China. Lower left: The alpine tundra in the study region, extending from 1850 to the summit at 2749 m (bottom). The red star represents the location of the climate station at the summit of the Changbai Mountains. The yellow line represents the international boundary between China and North Korea. Plots for ground truthing are indicated as green points. Right: field photos: (A) early autumn, 1 September 2017; (B) spring, 13 June 2017; and (C) early spring, 22 May 2015, showing the study site landscape at high

(above 2300 m), mid (2000-2300 m), and low elevations (1850-2000 m), respectively. Plant communities with green color in the field photos indicate *R. aureum* communities. Panel (B) shows *R. aureum* in white bloom. Plant communities with yellow and gray color are deciduous shrubs and sedge communities in (A) and herb communities in (B) and (C).

2.2 Workflow overview

To link *R. aureum* distribution changes to patterns in snow cover, we combined long-term satellite data from a variety of sources with other spatial datasets into two overarching models (Figure 2). We aimed to answer two questions: 1) is the spatial distribution of *R. aureum* distribution related to snow melting date? 2) are temporal changes in *R. aureum* distribution following changes in snow melting date? In what follows, we first describe all datasets and necessary image pre-processing, and then step by step elaborated the processes of 1) extracting spatial (a) and temporal (b) patterns in snow cover change; 2) extracting spatiotemporal patterns in *R. aureum* distribution; 3) establishing a model linking *R. aureum* distribution changes to snow cover change; 4) establishing a model to predict how future snowmelt dates will affect future distributions of *R. aureum*.

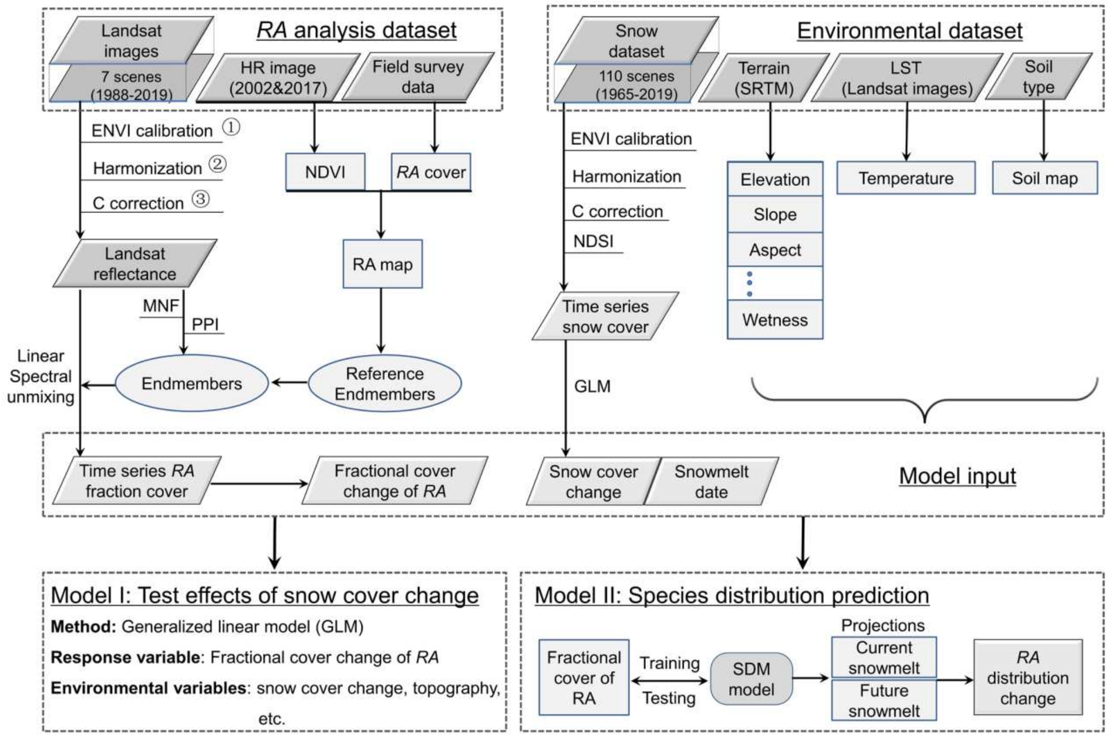

Figure 2. Schematic workflow that summarizes data preparation and processing steps, including the estimation of *Rhododendron aureum* fraction cover time series based on NDVI from Landsat images and high resolution images and field survey data (left), extraction of environmental data, most importantly the assessment of snow cover trends and snowmelt date based on various satellite datasets (right), and integration of both into two models for *R. aureum* (bottom). *RA* = *R. aureum*. HR refers to high resolution. PPI is the pixel purity index while MNF stands for minimum noise fraction transformation with ENVI. LST refers to land surface temperature derived from Landsat images. ① NDVI calibration includes orthorectification, atmospheric and radiometric calibrations; ② Harmonizations of multi-source images with ENVI; ③ C correction method for terrain correction.

2.3 Data collection and pre-processing

2.3.1 Climate data

Climate station data from 1959 to 2017 were obtained from the Tianchi weather station on the mountain summit from the Chinese meteorological data network (http://data.cma.gov.cn/, 42°10N, 128°50E, 2623 m, Figure 1). Quality control was performed to test data homogeneity using the RHtestV4 software (http://etccdi.pacificclimate.org/software.shtml).

2.3.2 Spring snow dataset

We collected multi-source satellite images with resolutions ranging from 0.8 m to 60 m that covered the entire snowmelt period (1 April to 15 June) from 1965 to 2019 (Supplementary Tab. 1). Six scenes of declassified KeyHole-4B data (1.83 m resolution) were acquired from the United States Geological Survey (USGS, http://edc.usgs.gov/), which uses Keyhole camera systems of the Corona satellite (a United States Department of Defense intelligence program, operative from 1959 to 1972). Other satellite images were 110 scenes of Landsat series (30 m resolution), two scenes of Pléiades-1 (0.8 m),across the archival satellite chronology (1978–2019) from the USGS website (http://glovis.usgs.gov). We removed all images with more than 50% cloud cover.

2.3.3 Autumn vegetation dataset

The end of the growing season in this alpine tundra is initiated late August, and snow onset occurs in early October (Zhang et al., 2010). We used a time window in autumn (September 20th to October 10th) for detecting the *R. aureum* distribution. Within this time window, *R. aureum*, as the only evergreen plant, is readily distinguishable from other plants, which are senesced (Fig. 3, a and b). Any green signal in that period thus corresponds largely to *R. aureum* presence, making it possible to use remote sensing to detect changes in its distribution over time. Finally, one scene of GF-2 satellite imagery (1 m resolution) obtained on 23 September 2017 (China Centre for Resource Satellite Data and Application, http://218.247.138.119:7777/DSSPlatform/index.html), one scene of IKONOS satellite image (1 m resolution) obtained on 20 September 2002, and 7 scenes of Landsat TM/ ETM+ imagery (1988–2019) were collected and used in this study (Supplementary Tab.1).

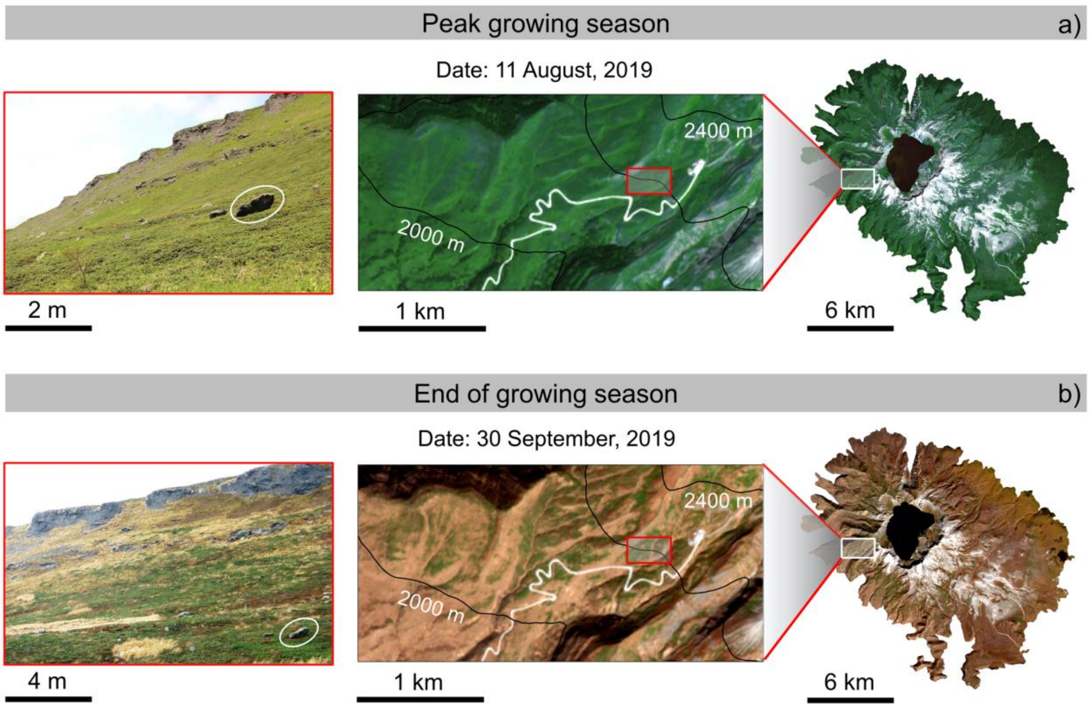

Figure 3. True color RGB image of Sentinel-2 (middle and right) and field photos (left) taken in the alpine tundra of the Changbai Mountains at peak (a) and end (b) of the

growing season. Green color at the end of the growing season represents the evergreen shrub, *R. aureum*; the white circle marks a distinctive rock for reference.

2.3.4 Image pre-processing

(1) Orthorectification calibration was applied to all high-resolution images (KeyHole-4B, Pléiades-1, and GF-2) through the Advanced World 3D (AW3D) data with high ground resolution (4.05 m), which was obtained in 2017 via the Advanced Land Observing Satellite (ALOS, http://www.eorc.jaxa.jp/ALOS). Specifically, we followed the method of Goossens et al. (2006) and Mihai et al. (2016) to eliminate the deformations and S-shaped distortion for the KeyHole-4B images.

(2) Radiometric calibration and atmospheric corrections were applied to all images based on ENVI tool platform (version 5.3). We applied terrain corrections following the method of Teillet et al., (1982) to eliminate illumination effects in rugged alpine terrain by using SRTM DEM (30 m resolution, http://glovis.usgs.gov). Digital numbers (DNs) of all Landsat images were converted into surface reflectance using the ENVI FLAASH module.

(3) Since the high-resolution images (KeyHole-4B, Pléiades-1, IKONOS, and GF-2) used in this study were cloud free, we used the Fmask method to extract cloud masks for Landsat images (Zhu et al., 2015). The normalized difference snow index (NDSI) itself could effectively discriminate snow and clouds (Hall 2012), which was a supplement for cloud masking.

(4) To homogenize multi-source images, we re-projected all images to WGS84

projection. Landsat series including MSS, TM, ETM+, and OLI sensors, accounted for 80% of our dataset. Spatial resolution and spectral reflectance of TM and ETM+ images, which were used for vegetation analysis in this study, remained unaltered.

2.4 Spring snow cover change

Step 1: *Snow cover extraction*

For the high-resolution images (KeyHole-4B and Pléiades-1), snow cover extent was extracted by using a supervised classification method combined with visual interpretation. For the Landsat data, snow cover extent was retrieved using NDSI (Hall, 2012). Pixels with NDSI values higher than 0.4 were classified as snow if their visible reflectances (Landsat band 3) were greater than 0.10 and their near-infrared reflectances (Landsat band 4) were greater than 0.11 (Dozier, 1989). The water body (i.e., Tianchi Lake at the top of the mountain) was masked from the final snow occurrence map.

Step 2: *Snow retrieval validation*

We did not use ground-level snow cover data for the validation of the derived snow cover because of its sparsity due to the remoteness and inaccessibility of the high mountain areas under study. However, studies showed that snow cover can be effectively validated using higher resolution images (Beck et al., 2005). To achieve this validation, we compared one pair of Pléiades-1 (0.8 m resolution, acquired on 1 June 2014) and Landsat-8 data (10 m resolution, acquired on 30 May 2014); showing a TSS statistic of 0.945. Overall, the snow identification ability of the coarser-grained satellite images used in this study was thus deemed sufficiently high.

Step 3: *Pixel level snow cover change and snowmelt date*

The snow occurrence data acquired from images with various resolutions (i.e., 1.83 m resolution from KeyHole-4B imagery and 30 m resolution from Landsat imagery) were first resampled to a pixel size of 30 m by using the Cubic convolution resampling method, which determines the new value of a cell based on fitting a smooth curve through the 16 nearest input cell centers (Shen and Tan 2020). Pixel level snow cover trend and snowmelt date was modelled using binomial generalized linear model (GLM) following Macander et al. (2015) and Niittynen and Luoto (2018). Every pixel had three strings of information that were passed as inputs for pixel-based GLMs: binary scores of snow occurrence (dependent variable); the corresponding year values (independent); and the corresponding DOY (day of year) values (independent). For the snow cover trend results, a positive trend represented increasing snow cover, while a negative trend represented decreasing snow cover. All of the image processing and statistics were performed in R environment (R Core Team) with the Raster package.

2.5 Distribution changes of *Rhododendron aureum*

2.5.1 Linear spectral unmixing

Spectral unmixing is a procedure which is implemented to decompose an image pixel into several constituents or endmembers (Ichoku and Karnieli 1996). An endmember is a pure surface material or land cover type that is assumed to have a unique spectral signature (Asis and Omasa 2007). As a widely used spectral unmixing method, the linear spectral unmixing model (LSUM) has proven to be effective in estimating endmember fractions due to its simplicity, interpretability, and high consistency for various land surface conditions (Small, 2003; Xiao and Moody, 2005; Yu et al., 2017). Two constraints were maintained in the LSUM: the fractions across all endmembers sum to one in a pixel, and each endmember fraction is in the range 0 to 1.

The LSUM assumed that (1) the spectral signature of a given pixel is the linear, proportion-weighted combination of the endmember spectra (Smith et al., 1990); and (2) each photon interacts only once with each endmember, without any non-linear processes (i.e. multiple scattering effect) involved (Cortés et al., 2014). The multiple scattering effect often occurs in areas with rugged ground surface, e.g., forested area or urban build-up, which may affect the accuracy of spectral unmixing (Dixit and Agarwal, 2021). The alpine tundra in this study area is distributed above the treeline, with vegetation composed of dwarf plant communities. We could thus ignore the bilinear mixing effects (i.e., interactions among components with different heights) in the unmixing process. To assess whether terrain complexity may affect our results, we analyzed terrain roughness at four resolutions (i.e., 5 m, 10 m, 15 m, and 30 m). We first calculated a roughness index (Riley et al., 1999) based on the AW3D DEM data with 5 m resolution data, and subsequently resampled the data to 10 m, 15 m, and 30 m resolutions in ArcGIS. We then applied a 30 m × 30 m window and calculated the variance of roughness of the pixels within that window. Theoretically, if terrain is rugged, the variance of roughness within a specific window should decrease as resolution increased. We however found that the variance of roughness did not decrease with increasing resolution from 5 m to 15 m (Supplementary Figure 1), indicating that the terrain is relatively uniform at the 30 m resolution and multiple scattering effects are limited in this study area.

Step 1: *Extraction of candidate endmembers*

The water body (the volcanic lake), cement road, and volcanic ash were excluded by determining pixels with NDVI < 0. Next, the most critical step in LSUM application is to find suitable endmembers to develop high quality fraction images. In this study, we combined the minimum noise fraction (MNF) transform algorithm and the pixel purity index (PPI) method to find the most spectrally pure pixels on the Landsat imagery. We used the MNF algorithm to determine the intrinsic data dimensionality and to separate signal from noise. The resulting data is represented in the MNF subspace and enclosed with a best-fitting simplex, the vertices of which are assumed to correspond with the component endmember (Ichoku and Karnieli 1996). Then we used the pixel purity index (PPI), the most commonly used method to find extremely pure pixels in multispectral images, to select candidate endmembers that are linearly independent (Boardman et al., 1995). The purest pixel in a given image is computed by repeatedly projecting n-D scatter plots on a random unit vector (Garg

2020). Both the MNF and PPI steps were conducted using ENVI software (version 5.3). In the end, candidate endmembers of *R. aureum* (representing greenness signal), deciduous shrubs (representing redness signal), and grasses (representing yellowness signal) were selected. The candidate endmembers of *R. aureum* were later evaluated by comparing to the reference endmembers in the next Step 2&3. The fraction cover of deciduous shrubs and grasses were no longer used.

Step 2: *Extraction of reference endmembers of* Rhododendron aureum

The high-resolution GF-2 image (25 September 2017) and IKONOS image (20 September 2002) were used to extract reference endmembers of *Rhododendron aureum*. In order to establish links between plot-level *R. aureum* cover and *R. aureum* occurrence on the high resolution imagery with a 1 m pixel size, we conducted field surveys at peak growing season and in autumn between 2014 and 2017, each year covering a different side of the mountain for logistical reasons. Three transects along the northern, western and southern sides of the mountain were set along the entire elevation range from 1850 to 2600 m. Each transect had a width of 200 m and included plots positioned at elevation intervals of 50 m. Four plots of 1 m^2 were established at each of the elevations, for a total of 192 plots across the three transects. The GPS location of each plot was measured using a handheld GPS (GARMIN GPS 60CX) with a horizontal error of 3 m. The abundance, height, and cover of each plant species inside the plots were recorded. Plant cover was calculated as the ratio of the area a species occupied divided by the sample plot size (1×1 m^2) and was measured using a frame (1×1 m^2 equally divided into 100 subplots) for each species in the field.

We then calculated the NDVI of the high resolution GF-2 image (25 September 2017) and IKONOS image (20 September 2002) with the following equation:

$$NDVI = (NIR-Red)/(NIR+Red) \quad (1)$$

where NIR and Red are the spectral reflectance in the near-infrared band and red band, respectively.

From the derived NDVI map, we extracted the NDVI values of locations of 165 field survey plot with *R. aureum* occurrences (plot size=1 m^2) and compared the NDVI values with the cover of *R. aureum* and herbs within these plots. Although the horizontal error (about 3 m) of the handheld GPS (GARMIN GPS 60CX) used during field work might have caused a mismatch between the 1 m resolution GF-2 image pixel and the 1 m^2 field survey plot, we still found a significant non-linear relationship between the NDVI greenness value and the plot-level *R. aureum* cover (Fig. 4), aided by the fact that most *R. aureum* patches were larger than 10 m in diameter. Autumn NDVI values and percent cover of *R. aureum* were indeed highly correlated (Figure 4). Ideally, when plant cover reaches 100%, NDVI equals 1. However, *R. aureum* is not a high leaf area plant, with extensive lateral branches occupying the space. Also, the GF-2 image was taken in late September, when *R. aureum* already passed its peak growth of the year. These factors may have resulted in a mismatch between NDVI and *R aureum* cover. Our predictive model suggests when *R. aureum* cover was greater than 90%, the NDVI value could reach 0.4, yet few higher NDVI values were observed (Figure 4). We can be 95% certain that NDVI-values of 0.4 or higher correspond with pixels with *R. aureum* cover of 90% or higher. Therefore, we set the NDVI threshold at 0.4, corresponding to a plot-level *R. aureum* cover of > 90%, and then extracted pixels which were treated as reference *R. aureum* endmembers (pixels purely occupied by this species with distinct spectral information).

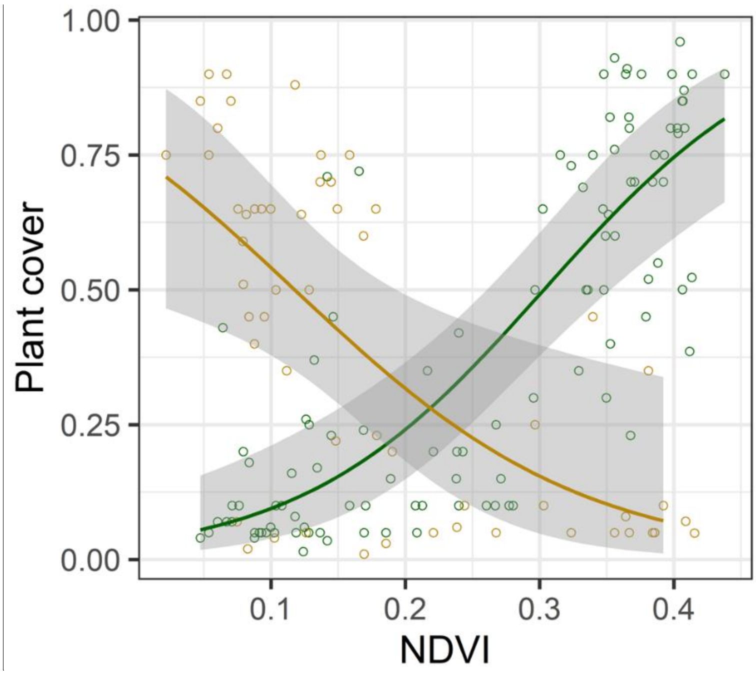

Figure 4. Correspondence between plant cover of *R. aureum* (green color) and herbs (brown color, as shown in Figure 1c) in 1 m^2 field survey plots and the NDVI value of a GF-2 high-resolution satellite image (23 September 2017, pixel size=1 m). Number of plots=165. The lines represent the results from generalized linear regressions (the *glm* function with 'logit' link from the 'MASS' package in R 2020). The grey zone indicates the 0.95 confidence interval.

Step 3: *Extract* Rhododendron aureum *distributions*

To further verify that the candidate *R. aureum* endmembers with 30 m resolution from Landsat imagery were sufficiently accurate for LUSM, the reference *R. aureum* endmembers from the 1 m resolution imagery (as identified with the field survey data) were compared to the candidate *R. aureum* endmembers (Asis and Omasa 2007). We abandoned candidate endmembers that mismatched reference endmembers (i.e., the candidate endmembers did not purely contain reference endmembers). Finally, three distinct endmembers were identified: the evergreen *R. aureum*, the deciduous shrubs, and the grasses (Supplementary Fig. 2). LUSM was then employed to extract *R. aureum* fractions from Landsat images about every 5 years (1988, 1992, 2001, 2004, 2009, 2013, and 2019). The whole process of linear spectral unmixing was conducted using the software ENVI (Version 5.3).

Step 4: *Validation of* Rhododendron aureum *distributions*

The *R. aureum* fraction images were assessed using the overall root-mean-square error (RMSE) of classification (Willmott, 1982). The lower the RMSE obtained, the higher unmixing accuracy was. For all Landsat images, RMSE were always lower than 3.9, indicating high unmixing accuracy (Supplementary Table 2). We conducted validation by using the aforementioned high-resolution images and the Landsat *R. aureum* fraction images (Suess et al., 2018). Specifically, the GF-2 image of 2017 and the IKONOS image of 2002 were used to validate the Landsat shrub fraction maps of 2019 and 2001, respectively. High resolution shrub abundance was calculated as the proportion of *R. aureum* footprints (i.e., 1-m resolution pixels identified as containing *R. aureum*) in each Landsat pixel (i.e., 30 × 30 m area). We statistically compared the estimated Landsat-based shrub cover fractions with the reference high resolution shrub abundance. As a measure of accuracy, we calculated the coefficient of determination ($R^2 = 0.982$) of the fitted linear regression model (Figure 5).

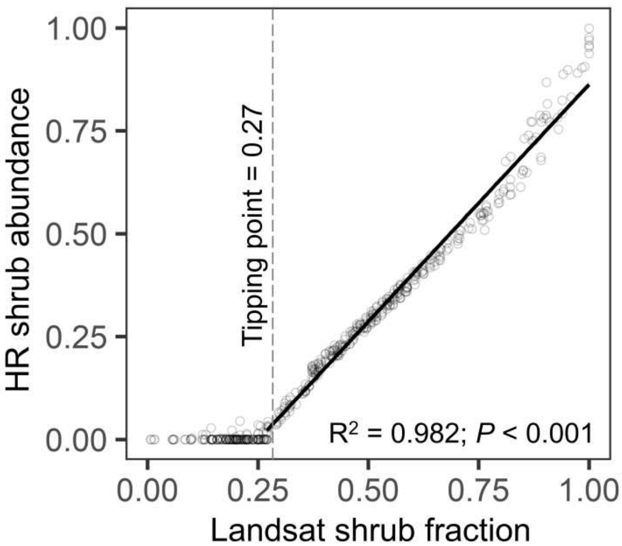

Figure 5. Scatterplot comparing Landsat shrub fraction to high resolution (HR) shrub abundance (the proportion of *R. aureum* footprints in each Landsat pixel). The black line represents the linear regression line fitting data that starts from the tipping point (0.27) onward.

2.5.2 Comparison with historical and current distributions of Rhododendron aureum

We selected *R. aureum* distributions in 1988 and 2019 as the historical and current distributions, respectively. By comparing high resolution image classification results, we found that biased estimations occurred for pixels with a low fraction of *R. aureum* cover, especially < 0.27 (Figure 5). Thus, we excluded non- *R. aureum* pixels from the *R. aureum* fraction images, for both 1988 and 2019. The fractional cover change of *R. aureum* was exhibited by using the differences of fraction cover of *R. aureum* between 2019 and 1988 (i.e., fraction cover of 2019 minus that of 1988). To verify this fraction cover change, *R. aureum* fraction dynamics computed from Landsat images taken at intervals of approximately 5 years were linked to and compared with changes we previously computed at the end years, 1988 and 2019.

2.6 Species distribution models (SDM)

To assess whether changes in *R. aureum* distribution follow changes in snow melting date in the context of climate warming, we modelled *R. aureum* distribution under current and future snowmelt scenarios. The current snowmelt scenario used the average snowmelt date derived from the GLM result from Section *2.3 Spring snow cover change*. As a simple theoretical advanced snowmelt scenario, we advanced snowmelt date by 5 days, as it has been observed that snow cover duration has declined on average by 5 days per decade in mountain ecosystems (Pörtner et al., 2019).

The fractional cover of *R. aureum* for the year 1988 was used as the response variable as this species was more likely in equilibrium with snow conditions in 1988 before rapid climate warming. Environmental predictive variables included one snow variable (i.e., the snowmelt date, supplementary Figure 5, a); one temperature variable (Land surface temperature data with 30 m resolution derived as the mean of four Landsat images covering the growing season from June to September in 2019 (downloaded from http://databank.casearth.cn). Landsat based LST data has been successfully applied in SDM studies even at fine spatial scale (He et al., 2015; Hernández-Lambraño et al., 2020), as such data can be sued to obtain synoptic, spatially continuous ecological values without interpolation or geographical biases at varying spatial and temporal resolutions (He et al., 2015). We applied Landsat based LST data because (1) weather stations are scarce is this region, (2) the widely used interpolated climate grids (e.g. WorldClim) are unlikely to capture fine spatial scale characteristics of the climate in mountain ecosystem (Fernandez et al., 2013), (3) the resolution of Landsat LST could well match other variables used in this study (all at 30 m resolution). Besides, we could also use LST data to focus on spatial variation of temperature during growing season. We also included one edaphic variable (30 m resolution, compiled using ArcGIS spatial analysis) derived from an earlier study (Zong et al., 2014) which identified the distribution of the two dominant types of soil (tundra soil and volcanic ash) in the region, and 11 topographic variables from the SRTM DEM data (30 m resolution), representing various ecological conditions that are known to have important effects on vegetation in our study area (Zong et al., 2014), using ArcGIS spatial analysis (Supplementary Table 3).

To eliminate multi-collinearity caused by the correlation among explanatory variables, only the variables with weak correlations (Pearson correlation coefficient < 0.3) were imported into the model (Zuur et al., 2010). Plane curvature, profile curvature, surface relief and roughness were thus excluded. Since spatial autocorrelation may inflate statistical significance due to the similarity between neighboring pixels, we applied the incremental spatial autocorrelation method (Lu et al., 2019) from the ArcGIS toolbox to determine the appropriate sampling distance (120 m) in this study.

We parameterized SDMs within the BIOMOD2 framework in the R modeling environment (Thuiller et al. 2009). To decrease the algorithm-based error, we applied four modelling methods (generalized linear model, GLM; multiple adaptive regression splines, MARS; flexible discriminant analysis, FDA; generalized boosted method, GBM). The GLMs were fitted including quadratic terms with a setting of interaction.level = 1. The GBMs were fitted using out-of-bag estimates of model improvement and the n.trees set as 1000. We used default settings for the MARS and FDA models. For each method, parameterization was replicated three times using random split-sampling (70% training and 30% evaluation). For each replicate, model accuracy was evaluated by means of the Area Under Curve (AUC) and the True Skill Statistic score (TSS). The models provide the probability of *R. aureum* for each cell that was then binarized by thresholding the probability according to a level that maximizes the TSS value of the predictions. In order to decrease the importance of a single modelling method, we applied the ensemble prediction method that judges that the species is present in a certain pixel if at least three of the four methods predicted an occurrence (Niittynen and Luoto, 2018).

2.7 Effects of snow cover change on the fractional cover change of *R. aureum*

We used a GLM to test the effects of snow cover change on the fractional cover change of *R. aureum*. As a response variable, we used the fractional cover change of *R. aureum* derived from section 2.5.2. Environmental predictive variables included one snow variable (i.e., snow cover trend derived from section 2.4, step 3), the aforementioned Land surface temperature and 11 topographic variables. We also conducted assessments of multi-collinearity and spatial autocorrelation. The statistics were performed in R (R Core Team) and ArcGIS environment.

3. Results

3.1 Spring snow cover change

The alpine tundra of the Changbai Mountains has warmed significantly at an average rate of 0.028 °C/year from 1959 to 2017 (P<0.001, Supplementary Fig. 3 and 4). Accordingly, snow cover decreased in most of the alpine tundra (Fig. 6) at elevations below 1950 m and in the elevation range of 2050 to 2250 m. An increasing trend of snow cover occurred not only at high elevations (above 2300 m) but also around an elevation of 2000 m. The average snowmelt date of our study area was 25 April (DOY = 115), ranging from mid-March (DOY = 78) to early June (DOY = 152). The snowmelt season thus lasts more than three months (Supplementary Fig. 5).

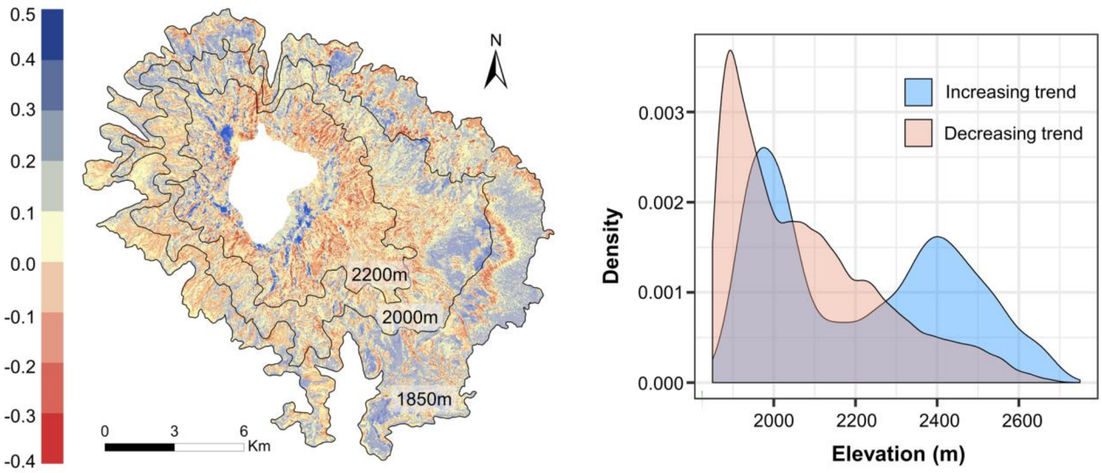

Figure 6. Pixel-level trends in snow cover (i.e., the coefficient of the 'year'-term in the generalized linear model) during the snowmelt period (1 April to 15 June) along elevation gradients in the alpine tundra of the Changbai Mountains from 1965 to 2019.

3.2 Distribution changes of *Rhododendron aureum*

During the past 30 years, the fraction cover of *R. aureum* experienced greater loss than gain (Tab. 1). The fractional changes of *R. aureum* cover were confirmed by the dynamic of *R. aureum* fraction cover at about five years' interval (Fig. 7). In general, fraction cover loss of *R. aureum* (8.66 km^2 area with cover loss of 50% or more and 10.29 km^2 of area with loss of -50% to -10%) was about twice as much as gain (5.57 km^2 of area with cover gain of +50% or more and 2.54 km^2 of area with gain of +10% to +50%) (Tab. 1).

Table 1. Change in fraction cover of *Rhododendron aureum* between 1988 and 2019

	Change in fraction cover of *Rhododendron aureum*				
Fractional change	< -50%	-50% – -10%	-10% – +10%	+10% – +50%	> +50%
Area (km^2)	8.66	10.29	3.45	2.54	5.57

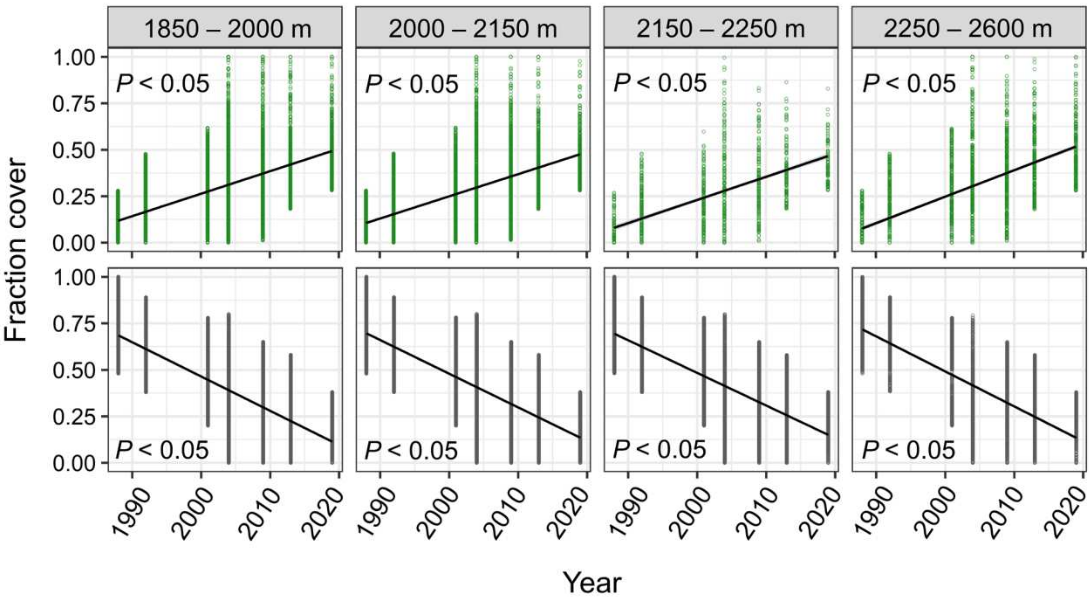

Figure 7. *R. aureum* fraction cover dynamics for increasing fraction cover (top four

panels) and decreasing cover (bottom four panels) pixels for the years 1988, 1992, 2001, 2004, 2009, 2013, and 2019.

Along the elevation gradient, *R. aureum* expanded at the leading edge (above 2300 m, Fig. 8) and retracted at the trailing edge (below 2000 m, Fig. 8). Interestingly, increasing and decreasing cover of *R. aureum* corresponded well with the increasing and decreasing trend of snow cover (Fig. 6) along the elevation gradient. This was confirmed by the GLM results (Tab. 2) indicating that the snow cover trend was the explanatory variable with the most influence on the change of fraction cover for *R. aureum*.

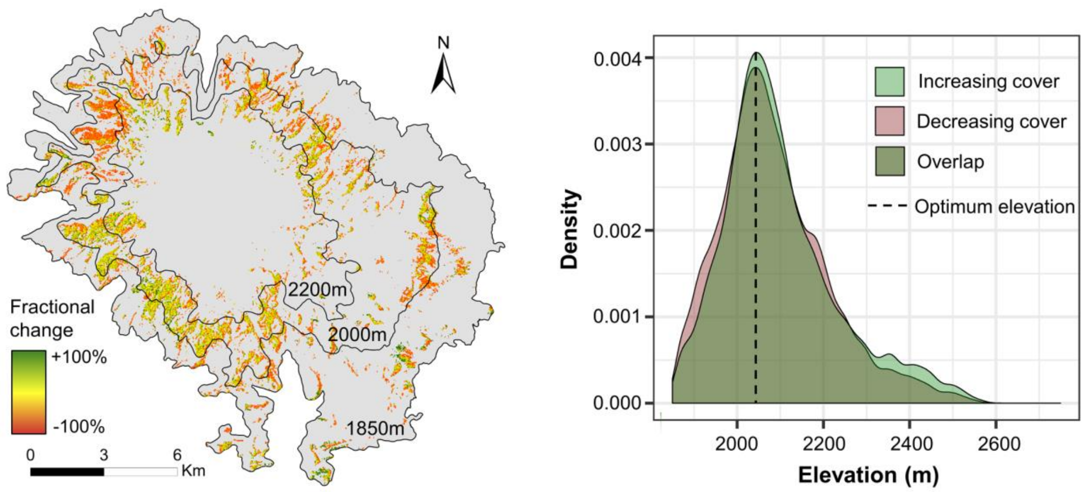

Figure 8. Change in fraction cover of *Rhododendron aureum* along elevation gradient between 1988 and 2019. Linear unmixing model was applied to extract fractional cover of *R. aureum* in 1988 and 2019.

Table 2. Results of the generalized linear model for predicting pixel-level change in fraction cover of *Rhododendron aureum* as a function of the snow cover trend, 8 topographic variables, and one temperature variable. Only variables that contributed

significantly (P<0.001) to the model fit were included in the final model. LST = Land surface temperature.

The change in fraction cover of *R. aureum*			
Variable	Coefficients	t value	*P*
Snow cover trend	**0.747**	6.097	***
LST	-0.017	-5.534	***
Slope	-0.001	-3.292	***
Aspect	0.001	16.232	***
Elevation	-0.0002	-10.261	***
Intercept	1.842	16.893	***

3.3 Distribution changes of *Rhododendron aureum* under future snowmelt scenarios

R. aureum preferred relatively late snowmelt regimes, with high occurrences predicted from DOY = 110 (i.e., 20 April) onwards (Fig. 9, a). Among various environmental variables (Fig. 9, b), snowmelt date was the most important predictor for *R. aureum* distribution, indicating a key role for snow in determining its distribution change. The species distribution models showed a good average model fit (area under curve (AUC) = 0.858; true skill statistics (TSS) = 0.578) for predicting *R. aureum* distribution (Supplementary Fig. 6). Our models suggested that, under a simplified future snowmelt scenario (i.e., five days advanced snowmelt across the whole study area), habitat loss of *R. aureum* could reach 75% (from 59.13 to 14.94 km^2, Fig. 10, c), especially at low elevations (Fig. 10, b). The optimum elevation of *R. aureum* moved to higher elevations under the future snowmelt scenario, indicating further upward range shifts of this shrub species in a climate with advanced snowmelt, when keeping all other factors constant (Fig. 10, d).

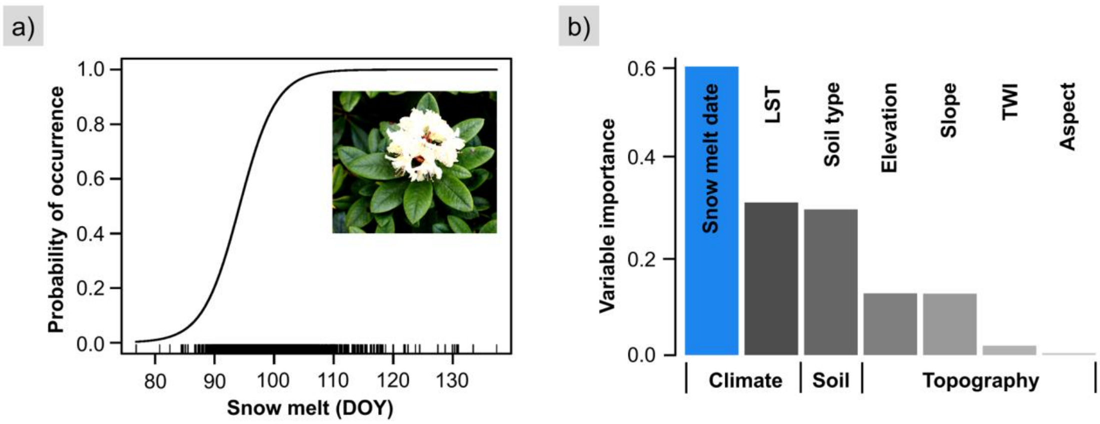

Figure 9. The snowmelt regime preference of the evergreen shrub, *Rhododendron aureum*. The response curve as a function of snowmelt day (DOY = day of year) is based on a generalized linear model. The vertical lines on the x-axis in a) indicate distribution density of *R. aureum*. The variable importance scores are mean values from all four species distribution modelling methods. LST indicates land surface temperature derived from Landsat imagery. TWI indicates topographical wetness index.

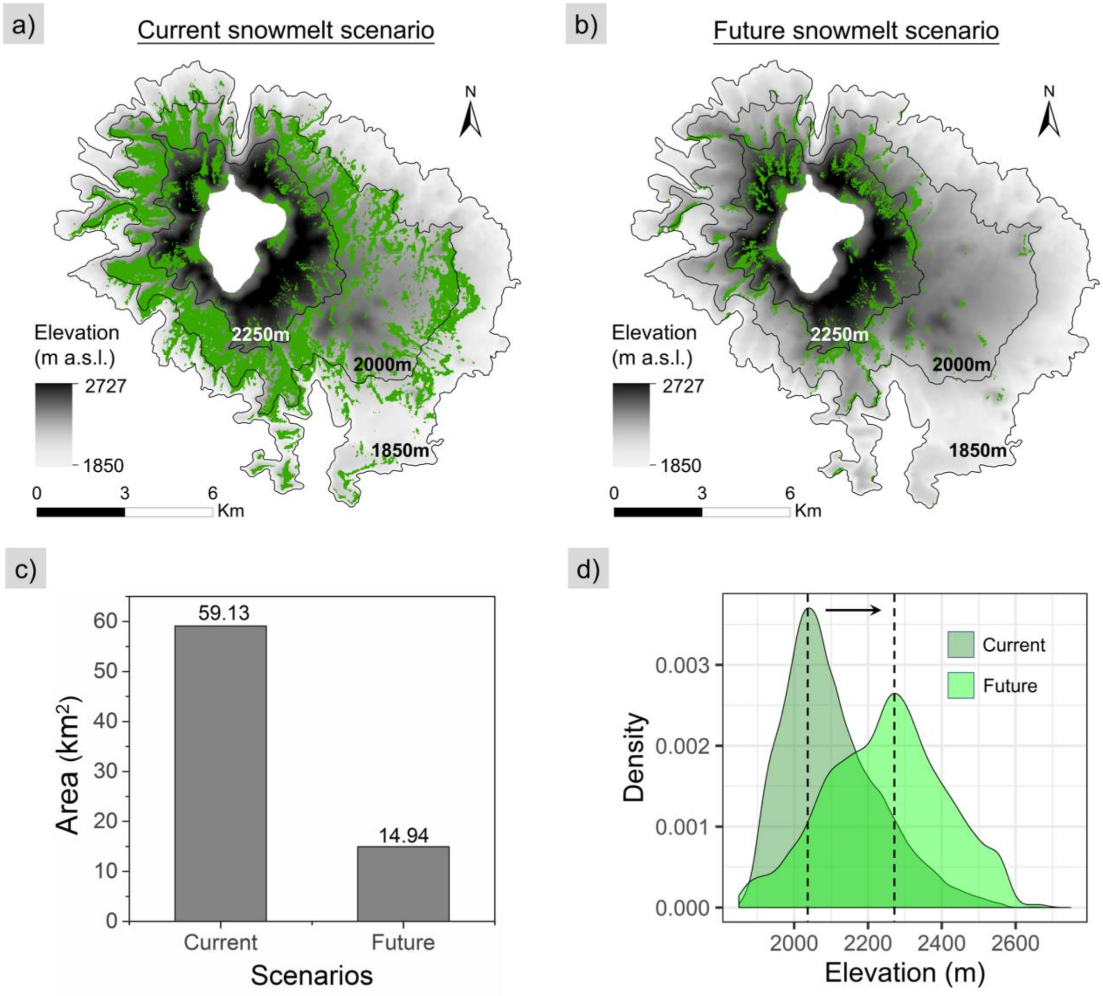

Figure 10. The projected distributions of *Rhododendron aureum* (represented in green) under current (a) and future snowmelt scenarios (b) based on a species distribution model. The number of pixels (c) and distribution frequencies along the elevation gradient (d) of *R. aureum* as predicted under scenarios for the current snowmelt regime and a future regime. The dashed lines indicate the elevation optimum in each scenario.

4. Discussion

4.1 Half a century of spring snow cover change

Warming in the alpine tundra of the Changbai Mountains (0.0278 °C/year during the period 1959 to 2017) has been comparable to trends observed for other mountains in the northern hemisphere over similar periods, e.g., in North America (0.035 °C/year on Mt. Washington, NH, USA), the European Alps (0.03 °C/year on Mt. Sonnblick, Austria) and Asia (0.035 °C/year on Mt. Fuji, Japan) (Pörtner et al., 2019). In line with the warming trend, snow cover during snowmelt period (1 April to 15 June) showed a decreasing trend for most of the study area during the last 50 years, which supported the recent assessment report about the cryosphere indicating that mountain snow cover has declined remarkably and globally (Pörtner et al., 2019). In general, fine-scale remote sensing records are considered insufficiently long to assess alpine snow cover trends (Bormann et al., 2018). However, by taking advantage of the declassified high-resolution KeyHole data starting in the 1960s, we demonstrate a practical way to build a snow dataset for alpine areas spanning over half a century. Snow classification accuracies of the images employed in this study were > 0.94, much higher than those from combined mid- and coarse-resolution datasets (Dietz et al., 2012). The resolution discrepancy between high- and mid-resolution data was $<$ 30 m, much lower than those ($>$ 200 m) between mid- and coarse-resolution data. Thus, this dataset could match fine-scale snow cover change in heterogeneous alpine landscapes much more closely than previous alpine snow datasets with a hundred-meter level resolution (Molotch and Margulis, 2008; Wan et al., 2014; Wang et al., 2017).

To the best of our knowledge, the snow dataset we built was the first one based on remote sensing to span 50 years for alpine ecosystems. Other alpine snow products exist, such as simulated potential snow accumulation patterns calculated from topographic data (Gottfried et al., 1998; Randin et al., 2009), first snow-free day extracted from multiple satellite datasets (Dedieu et al., 2016), predicted snow cover duration of 5 years derived from the Landsat dataset (Carlson et al., 2015), or snow cover duration (SCD) derived from the SPOT satellite for a period of less than 20 years (Dirnböck et al., 2003). All of these snow products emphasized the importance of snow in explaining vegetation distributions in cold biomes. The spring snowmelt period is probably ecologically more relevant than the snow onset in autumn, as earlier snowmelt has been found to contribute more to a reduction in SCD than late snow onset (Klein et al., 2016) and is potentially correlated with the number of freezing days experienced by plants in spring, as well as with growing season length (Winkler et al., 2018). The main limitation of our snow dataset may be that the snow variable used here does not incorporate snow depth, although snow depth has been shown to correlate with SCA in alpine terrain. From this perspective, proper utilization of synthetic aperture radar data was recommended as auxiliary data. However, there is always a trade-off between long timespan and high temporal resolution when analyzing snow dynamics. Nevertheless, further investigation of the links between snow cover area, snow depth and snowmelt data could prove useful for understanding (changes in) plant species distributions (Falk et al., 2016).

4.2 Links between snow cover and distribution changes of *Rhododendron aureum*

We found that snowmelt date was the most important predictor for *R. aureum* distribution, indicating the important role of snow in determining persistence of this shrub species in a warming climate. Using an SDM approach, we obtained the snow response curve of *R. aureum* and identified its preferred snowmelt regime as those habitats with snowmelt date starting from 20 April. This analysis supports previous findings that *R. aureum* is not a typical frost-tolerant alpine species, yet that it requires snow cover protection from extreme low temperatures to survive in this alpine tundra (Liu et al., 2009; Zhang et la., 2010). *R. aureum* preferred relatively late snow cover conditions, indicating that their distribution is prone to be affected as climate – and thus snowmelt dates – changes. Indeed, we have observed changes in *R. aureum* distribution following snow cover changes over the last decades. Our models suggested that *R. aureum* would further shift the distribution range to higher elevations under an advanced snowmelt scenario, results in line with field observations and model predictions that alpine plant species shift their ranges to higher elevations, with losses at their trailing edge in response to the warming climate (Gottfried et al., 2012; Lenoir et al., 2008; Rixen and Wipf, 2017; Sandvik and Odland, 2014). Furthermore, the distribution area of *R. aureum* would reduce by 75%, a number significantly higher than the projections for the end of the twenty-first century (33–55%) from model predictions for alpine plant species in the European Alps (Dullinger et al., 2012). Note, however, that this is a theoretical prediction under a largely simplified scenario in which all other global change factors (e.g., other influences of temperature and precipitation change) are kept constant.

Range shifts of alpine plant species under environmental change are driven by two major processes: the extinction of existing populations at sites that have become unsuitable and the colonization of sites that become newly suitable (Rumpf et al., 2019). The reduced snow cover area in the Changbai Mountains probably caused the loss of *R. aureum* at the trailing edge. At the leading edge, *R. aureum* colonized areas with deep snow cover, indicating that the currently snow-rich habitats might be suitable sites for *R. aureum* in a warmer climate. Early snowmelt can expose shrubs to lower spring temperatures and increase the risk of frost damage (Wipf et al., 2006). Indeed, the European *Rhododendron ferrugineum* has been shown to rely on snow cover for protection from frost (Francon et al., 2020). Snow habitats hence provide microrefugia, buffering against frost damage and protecting *Rhododendron* at higher elevations. One limitation of our SDMs is that we don't have fine resolution temperature data to match the snowmelt change, which is due to the lack of evenly distributed and long term *in situ* temperature observations in this alpine tundra, as it has been found that high resolution spatial temperature information is helpful to predict biodiversity change in cold biome (Niittynen et al., 2018). We thus recommend further investigation of long-term and fine scale temperature observations for understanding (changes in) plant distributions in alpine ecosystems (Lembrechts et al., 2019).

Other possible mechanisms underlying *R. aureum* distribution change could be related to summer warming or drought as observed in many arctic and alpine ecosystems (Berner et al., 2020). However, summer precipitation is fairly high in this alpine tundra (about 960 mm for four months), and hence might not be the limiting factor for *R. aureum* growth. Nevertheless, tree-ring analysis might be a possibility to disentangle the effects of summer warming and snow cover change. Other causes such as disturbances are minimal since the area has practically no access for humans, and there have been no other reported natural disturbances for the past decades.

4.3 Distribution changes of *R. aureum* over last decades

The main novelty of our study is that we used the species-specific phenology of the evergreen shrub *R. aureum* to identify its cover. We extracted its historical and current fraction cover distributions from Landsat images by taking advantage of *R. aureum*'s greenness in autumn compared with the brownness of surrounding plants in this study system. The combination of plot-scale field data and the GF-2 image with a pixel size of 1 m provided sufficient and effective endmembers for the linear unmixing analysis. In a similar study, Tape et al. (2006) applied repeated high-resolution aerial photographs to document shrub expansion in the Alaskan Arctic. In the same region, shrubs could be accurately identified at the treeline ecotone, where they usually exhibited textures (e.g., high plant height) distinctive from those of the surrounding vegetation in imagery (Selkowitz, 2010). However, our study provides an approach to extracting shrubs beyond the treeline by focusing on phenological anomalies of shrubs rather than texture, thus introducing a novel way to study shrub distribution changes in inner Arctic or alpine ecosystems (Bayle et al., 2019; van Lier et al., 2009). Phenological differences in autumn between shrubs and other plant functional types have long been neglected. So far, using phenology to identify plant cover has been applied to map expansion processes of invasive plants (Bradley, 2014; Peterson, 2005; Weisberg et al., 2017). We identified only one study in which shrubland in the French Alps was successfully extracted by using the specific phenology of reddening shrubs in autumn based on the red edge band of Sentinel-2 data (Bayle et al., 2019).

Expansion of deciduous shrubs, such as birch (Betula spp.), willow (Salix spp.), and alder (Alnus spp.), through infilling of existing patches, an increase in growth, or an advancing shrubline, i.e., shrubification, was found to contribute to the vegetation change during past decades (Myers-Smith et al., 2011). However, there is evidence that evergreen shrubs (e.g., crowberry) are also expanding (Elmendorf et al., 2012; Klanderud and Birks, 2003; Maliniemi et al., 2018; Vowles and Björk, 2019; Vuorinen et al., 2017; Wilson and Nilsson, 2009). Thus, the approach introduced in our study is a promising way to extract the distribution of these evergreen shrubs, if they are abundant, in Arctic and alpine ecosystems by using autumn NDVI signals. This knowledge in turn can contribute to an improved understanding of shrub distribution changes and help to address the complexities of interpreting satellite-spectral and ground-vegetation greening trends (Myers-Smith et al., 2020). It should be noted that phenology shift due to climate warming might affect the detection of specific species especially in alpine ecosystems with sharp environmental gradients in elevation and topography (Gottfried et al., 1998). However, warming mostly advanced or delayed the die-off of other perennial plants by less than a week during the past 30 years (Liu et al., 2016), suggesting that warming-caused phenology change should not affect the detection of *R. aureum* in this study, which had a window of several weeks for successful detection due to its unique greenness in autumn. Nevertheless, field phenology observation along elevation gradient could be a good supplementary to the selection of proper satellite imagery.

Acknowledgments

This work was supported by the National Key R & D Program of China [grant numbers 2019YFC0409101, 2016YFA0602301]; the National Natural Science Foundation of China [grant number 41971124]; the Natural Science Foundation of Jilin Scientific Institute of China [grant number 20180520087JH]; and the University of GIS Missouri Mission Enhancement Program. JJL is funded by the Research Foundation Flanders (FWO, grant number 12P1819N). The authors are much appreciating Nathalie Chardon's help in statistics, Ming Li's help in Landsat data processing, and field assistance from Kai Liu, Xinyuan Tan, and Miaomiao Wu. We thank Melissa Dawes and Steve Shifley for help with language improvement.

References

Asis, A. M., & Omasa, K. (2007). Estimation of vegetation parameter for modeling soil erosion using linear Spectral Mixture Analysis of Landsat ETM data. *ISPRS Journal of Photogrammetry and Remote Sensing*, *62(4)*, 309-324. DOI: 10.1016/j.isprsjprs.2007.05.013

Bayle, A., Carlson, B.Z., Thierion, V., Isenmann, M., & Choler, P. (2019). Improved mapping of mountain shrublands using the sentinel-2 red-edge band. *Remote Sensing*, *11*, 2807. DOI: 10.3390/rs11232807

Beamish, A., Raynolds, M.K., Epstein, H., Frost, G.V., Macander, M.J., Bergstedt, H., Bartsch, A., Kruse, S., Miles, V., & Tanis, C.M. (2020). Recent trends and remaining challenges for optical remote sensing of Arctic tundra vegetation: A review and outlook. *Remote Sensing of Environment*, *246*, 111872. DOI: 10.1016/j.rse.2020.111872

Beck, P.S., Kalmbach, E., Joly, D., Stien, A., & Nilsen, L. (2005). Modelling local distribution of an Arctic dwarf shrub indicates an important role for remote sensing of snow cover. *Remote Sensing of Environment*, *98*, 110-121. DOI: 10.1016/j.rse.2005.07.002

Berner, L.T., Massey, R., Jantz, P., Forbes, B.C., Macias-Fauria, M., Myers-Smith, I., Kumpula, T., Gauthier, G., Andreu-Hayles, L., & Gaglioti, B.V. (2020). Summer warming explains widespread but not uniform greening in the Arctic tundra biome. *Nature Communications*, *11*, 1-12. DOI: https://doi.org/10.1038/s41467-020-18479-5

Billings, W.D., & Bliss, L. (1959). An alpine snowbank environment and its effects on vegetation, plant development, and productivity. *Ecology*, *40*, 388-397. DOI: 10.2307/1929755

Boardman, J., Kruse, F.A., & Green, R. (1995). Mapping target signatures via partial unmixing of AVIRIS data. In Summaries of the Fifth Annual JPL Airborne Earth Science Workshop. In (pp. 23–26). United States: JPL Publication

Bokhorst, S., Pedersen, S.H., Brucker, L., Anisimov, O., Bjerke, J.W., Brown, R.D., Ehrich, D., Essery, R.L., Heilig, A., & Ingvander, S. (2016). Changing Arctic snow cover: A review of recent developments and assessment of future needs for observations, modelling, and impacts. *Ambio*, *45*, 516-537. DOI: 10.1007/s13280-016-0770-0

Bormann, K.J., Brown, R.D., Derksen, C., & Painter, T.H. (2018). Estimating snow-cover trends from space. *Nature Climate Change*, *8*, 924-928. DOI: 10.1038/s41558-018-0318-3

Bradley, B.A. (2014). Remote detection of invasive plants: a review of spectral, textural and phenological approaches. *Biological Invasions*, *16*, 1411-1425. DOI: 10.1007/s10530-013-0578-9

Carbognani, M., Tomaselli, M., & Petraglia, A. (2014). Current vegetation changes in an alpine late snowbed community in the south-eastern Alps (N-Italy). *Alpine Botany*, *124*, 105-113. DOI: 10.1007/s00035-014-0135-x

Carlson, B.Z., Choler, P., Renaud, J., Dedieu, J.-P., & Thuiller, W. (2015). Modelling snow cover duration improves predictions of functional and taxonomic diversity for alpine plant communities. *Annals of Botany*, *116*, 1023-1034. DOI: 10.1093/aob/mcv041

Carlson, B.Z., Corona, M.C., Dentant, C., Bonet, R., Thuiller, W., & Choler, P. (2017). Observed long-term greening of alpine vegetation—a case study in the French Alps. *Environmental Research Letters*, *12*, 114006. DOI: 10.1088/1748-9326/aa84bd

Carlson, B.Z., Randin, C.F., Boulangeat, I., Lavergne, S., Thuiller, W., & Choler, P. (2013). Working toward integrated models of alpine plant distribution. *Alpine Botany*, *123*, 41-53. DOI: 10.1007/s00035-013-0117-4

Cooper, E.J., Dullinger, S., & Semenchuk, P. (2011). Late snowmelt delays plant development and results in lower reproductive success in the High Arctic. *Plant Science*, *180*, 157-167. DOI: 10.1016/j.plantsci.2010.09.005

Cooper, E.J., Little, C.J., Pilsbacher, A.K., & Mörsdorf, M.A. (2019). Disappearing green: Shrubs decline and bryophytes increase with nine years of increased snow accumulation in the High Arctic. *Journal of Vegetation Science*, *30*, 857-867. DOI: 10.1111/jvs.12793

Cortés, G., Girotto, M., & Margulis, S. A. (2014). Analysis of sub-pixel snow and ice extent over the extratropical Andes using spectral unmixing of historical Landsat imagery. *Remote sensing of environment*, *141*, 64-78. DOI: 10.1016/j.rse.2013.10.023

Daniëls, F.J.A., De Molenaar, J.G., Chytrý, M., & Tichý, L. (2015). Vegetation change in Southeast Greenland? Tasiilaq revisited after 40 years. *Applied Vegetation Science*, *14*, 230-241. DOI: 10.1111/j.1654-109X.2010.01107.x

Dedieu, J.-P., Carlson, B.Z., Bigot, S., Sirguey, P., Vionnet, V., & Choler, P. (2016). On the importance of high-resolution time series of optical imagery for quantifying the effects of snow cover duration on alpine plant habitat. *Remote Sensing*, *8*, 481. DOI: 10.3390/rs8060481

Dietz, A.J., Kuenzer, C., Gessner, U., & Dech, S. (2012). Remote sensing of snow–a review of available methods. *International Journal of Remote Sensing*, *33*, 4094-4134. DOI: 10.1080/01431161.2011.640964

Dirnböck, T., Dullinger, S., & Grabherr, G. (2003). A regional impact assessment of climate and land‐use change on alpine vegetation. *Journal of Biogeography*, *30*, 401-417. DOI: 10.1046/j.1365-2699.2003.00839.x

Dixit, A., & Agarwal, S. (2021). on-linear Spectral Unmixing of Hyperspectral Data using Modified PPNMM. *Applied Computing and Geosciences*, *9(8)*, 100053. DOI: https://doi.org/10.1016/j.acags.2021.100053

Dozier, J. (1989). Spectral signature of alpine snow cover from the Landsat Thematic Mapper. *Remote sensing of environment*, *28*, 9-22. DOI: 10.1016/0034-4257(89)90101-6

Dullinger, S., Gattringer, A., Thuiller, W., Moser, D., Zimmermann, N.E., Guisan, A., Willner, W., Plutzar, C., Leitner, M., & Mang, T. (2012). Extinction debt of high-mountain plants under twenty-first-century climate change. *Nature Climate Change*, *2*, 619-622. DOI: 10.1038/nclimate1514

Elmendorf, S.C., Henry, G.H., Hollister, R.D., Björk, R.G., Boulanger-Lapointe, N., Cooper, E.J., Cornelissen, J.H., Day, T.A., Dorrepaal, E., & Elumeeva, T.G. (2012). Plot-scale evidence of tundra vegetation change and links to recent summer warming. *Nature Climate Change*, *2*, 453-457. DOI: 10.1038/nclimate1465

Falk, U., Gieseke, H., Kotzur, F., & Braun, M. (2016). Monitoring snow and ice surfaces on King George Island, Antarctic Peninsula, with high-resolution TerraSAR-X time series. *Antarctic Science*, *28*, 135-149. DOI: 10.1017/S0954102015000577

Fernandez, M., Hamilton, H. & Kueppers, L.M. (2013) Characterizing uncertainty in species distribution models derived from interpolated weather station data. *Ecosphere*, **4**, art. 61. DOI: 10.1890/ES13-00049.1

Filippa, G., Cremonese, E., Galvagno, M., Isabellon, M., Bayle, A., Choler, P., Carlson, B.Z., Gabellani, S., Morra di Cella, U., & Migliavacca, M. (2019). Climatic drivers of greening trends in the Alps.

Remote Sensing, *11*, 2527. DOI: 10.3390/rs11212527

Forbes, B.C., Fauria, M.M., & Zetterberg, P. (2010). Russian Arctic warming and 'greening' are closely tracked by tundra shrub willows. *Global Change Biology*, *16*, 1542-1554. DOI: 10.1111/j.1365-2486.2009.02047.x

Formica, A., Farrer, E.C., Ashton, I.W., & Suding, K.N. (2014). Shrub expansion over the past 62 years in Rocky Mountain alpine tundra: possible causes and consequences. *Arctic, Antarctic, and Alpine Research*, *46*, 616-631. DOI: 10.1657/1938-4246-46.3.616

Francon, L., Corona, C., Till-Bottraud, I., Choler, P., Carlson, B., Charrier, G., Améglio, T., Morin, S., Eckert, N., & Roussel, E. (2020). Assessing the effects of earlier snow melt-out on alpine shrub growth: The sooner the better? *Ecological Indicators*, *115*, 106455. DOI: 10.1016/j.ecolind.2020.106455

Garg, P. K. (2020). Effect of contamination and adjacency factors on snow using spectroradiometer and hyperspectral images. *Hyperspectral Remote Sensing*, 167-196. DOI: 10.1016/B978-0-08-102894-0.00016-4

Gerdol, R., Siffi, C., Iacumin, P., Gualmini, M., & Tomaselli, M. (2013). Advanced snowmelt affects vegetative growth and sexual reproduction of *Vaccinium myrtillus* in a sub - alpine heath. *Journal of Vegetation Science*, *24*, 569-579. DOI: 10.1111/j.1654-1103.2012.01472.x

Good, M., Morgan, J.W., Venn, S., & Green, P. (2019). Timing of snowmelt affects species composition via plant strategy filtering. *Basic and Applied Ecology*, *35*, 54-62. DOI: 10.1016/j.baae.2019.01.004

Goossens, R., De Wulf, A., Bourgeois, J., Gheyle, W., & Willems, T. (2006). Satellite imagery and archaeology: the example of CORONA in the Altai Mountains. *Journal of Archaeological Science*, *33*, 745-755. DOI: 10.1016/j.jas.2005.10.010

Gottfried, M., Pauli, H., Futschik, A., Akhalkatsi, M., Barančok, P., Alonso, J.L.B., Coldea, G., Dick, J., Erschbamer, B., & Kazakis, G. (2012). Continent-wide response of mountain vegetation to climate change. *Nature Climate Change*, *2*, 111-115. DOI: 10.1038/nclimate1329

Gottfried, M., Pauli, H., & Grabherr, G. (1998). Prediction of vegetation patterns at the limits of plant life: a new view of the alpine-nival ecotone. *Arctic and Alpine Research*, *30*, 207-221. DOI: 10.2307/1551968. DOI: 10.2307/1551968

Greaves, H.E., Vierling, L.A., Eitel, J.U., Boelman, N.T., Magney, T.S., Prager, C.M., & Griffin, K.L. (2016). High-resolution mapping of aboveground shrub biomass in Arctic tundra using airborne lidar and imagery. *Remote Sensing of Environment*, *184*, 361-373. DOI: 10.1016/j.rse.2016.07.026

Hall, D. (2012). *Remote sensing of ice and snow*. Springer Science & Business Media. DOI: 10.1007/978-94-009-4842-6

Hallinger, M., Manthey, M., & Wilmking, M. (2010). Establishing a missing link: warm summers and winter snow cover promote shrub expansion into alpine tundra in Scandinavia. *New Phytologist*, *186*, 890-899. DOI: 10.1111/j.1469-8137.2010.03223.x

Heegaard, E. (2002). A model of alpine species distribution in relation to snowmelt time and altitude. *Journal of Vegetation Science*, *13*, 493-504. DOI: 10.1111/j.1654-1103.2002.tb02076.x

He, K. S., Bradley, B. A., Cord, A. F., Rocchini, D., Tuanmu, M.-N., Schmidtlein, S., … Pettorelli, N. (2015). Will remote sensing shape the next generation of species distribution models? *Remote Sensing in Ecology and Conservation, 1*, 4–18. DOI: https://doi.org/10.1002/rse2.7

Hiemstra, C.A., Liston, G.E., & Reiners, W.A. (2002). Snow redistribution by wind and interactions with vegetation at upper treeline in the Medicine Bow Mountains, Wyoming, USA. *Arctic, Antarctic, and Alpine Research*, *34*, 262-273. DOI: 10.2307/1552483

Hughes, N.M. (2011). Winter leaf reddening in ‘evergreen’ species. *New Phytologist*, *190*, 573-581. DOI: 10.1111/j.1469-8137.2011.03662.x

Ichoku, C., & Karnieli, A. (1996). A review of mixture modeling techniques for sub‐pixel land cover estimation. *Remote sensing reviews*, *13(3-4)*, 161-186. DOI: 10.1080/02757259609532303Keller, F., Goyette, S., & Beniston, M. (2005). Sensitivity analysis of snow cover to climate change scenarios and their impact on plant habitats in alpine terrain. *Climatic Change*, *72*, 299-319. DOI: 10.1007/s10584-005-5360-2

Klanderud, K., & Birks, H.J.B. (2003). Recent increases in species richness and shifts in altitudinal distributions of Norwegian mountain plants. *The Holocene*, *13*, 1-6. DOI: 10.1191/0959683603hl589ft

Klein, G., Vitasse, Y., Rixen, C., Marty, C., & Rebetez, M. (2016). Shorter snow cover duration since 1970 in the Swiss Alps due to earlier snowmelt more than to later snow onset. *Climatic Change*, *139*, 637-649. DOI: 10.1007/s10584-016-1806-y

Kudo, G. (1991). Effects of snow-free period on the phenology of alpine plants inhabiting snow patches. *Arctic and alpine research*, *23(4)*, 436-443. DOI: 10.2307/1551685

Kudo, G. (1993). Relationship between flowering time and fruit set of the entomophilous alpine shrub, *Rhododendron aureum* (Ericaceae), inhabiting snow patches. *American Journal of Botany*, *80*, 1300-1304. DOI: 10.2307/2445714

Kudo, G., & Ito, K. (1992). Plant distribution in relation to the length of the growing season in a snow-bed in the Taisetsu Mountains, northern Japan. *Vegetatio*, *98(2)*, 165-174. DOI: 10.1007/BF00045554

Labonté, J., Drolet, G., Sylvain, J.-D., Thiffault, N., Hébert, F., & Girard, F. (2020). Phenology-based mapping of an alien invasive species using time series of multispectral satellite data: a case-study with Glossy Buckthorn in Québec, Canada. *Remote Sensing*, *12*, 922. DOI: 10.3390/rs12060922

Lembrechts, J. J. , Lenoir, J. , Roth, N. , Hattab, T. , & Nijs, I. . (2019). Comparing temperature data sources for use in species distribution models: from in‐situ logging to remote sensing. *Global Ecology and Biogeography*, *28*, 1578–1596. DOI: https://doi.org/10.1111/geb.12974

Lenoir, J., Gégout, J.C., Marquet, P.A., De, R.P., & Brisse, H. (2008). A significant upward shift in plant species optimum elevation during the 20th century. *Science*, *320*, 1768-1771. DOI: 10.1126/science.1156831

Liu, Q. , Fu, Y. H. , Zhu, Z. , Liu, Y. , Liu, Z. , & Huang, M. , et al. (2016). Delayed autumn phenology in the northern hemisphere is related to change in both climate and spring phenology. *Global Change Biology*, *22(11)*, 3702-3711. DOI: info:doi/10.1111/gcb.13311

Liu, Q., Xu, Q., & Zhang, G. (2009). Impact of alpine snowpacks on primary productivity in *Rhododendron aureum* community in Changbai Mountains, China. *Acta Ecologica Sinica, 29*, 4035-4044. DOI: 10.1007/978-1-4020-9623-5_5 (In Chinese)

Liu, R., Wei, H., & Li, J. (1998). *Modern eruption of Changbaishan Tianchi volcano*. Beijing, China: Science Press (In Chinese)

Lu, P., Bai, S., Tofani, V., & Casagli, N. (2019). Landslides detection through optimized hot s pot analysis on persistent scatterers and distributed scatterers. *ISPRS Journal of Photogramm etry and Remote Sensing*, *156*, 147-159. DOI: 10.1016/j.isprsjprs.2019.08.004

Macander, M. J., Swingley, C. S., Joly, K., & Raynolds, M. K. (2015). Landsat-based snow pe rsistence map for northwest Alaska. *Remote Sensing of Environment*, *163*, 23-31. DOI: 10.1 016/j.rse.2015.02.028

Macias-Fauria, M., Forbes, B.C., Zetterberg, P., & Kumpula, T. (2012). Eurasian Arctic greening reveals teleconnections and the potential for structurally novel ecosystems. *Nature Climate Change*, *2*, 613-618. DOI: 10.1038/NCLIMATE1558

Malfasi, F., & Cannone, N. (2020). Climate warming persistence triggered tree ingression after shrub encroachment in a high alpine tundra. *Ecosystems*, 1-19. DOI: 10.1007/s10021-020-00495-7

Maliniemi, T., Kapfer, J., Saccone, P., Skog, A., & Virtanen, R. (2018). Long‐term vegetation changes of treeless heath communities in northern Fennoscandia: Links to climate change trends and reindeer grazing. *Journal of Vegetation Science*, *29*, 469-479. DOI: 10.1111/jvs.12630

Mallik, A.U., Wdowiak, J.V., & Cooper, E.J. (2011). Growth and reproductive responses of *Cassiope tetragona*, a circumpolar evergreen shrub, to experimentally delayed snowmelt. *Arctic, Antarctic, and Alpine Research*, *43*, 404-409. DOI: 10.1657/1938-4246-43.3.404

Martin, A.C., Jeffers, E.S., Petrokofsky, G., Myers-Smith, I., & Macias-Fauria, M. (2017). Shrub growth and expansion in the Arctic tundra: an assessment of controlling factors using an evidence-based approach. *Environmental Research Letters*, *12*, 085007. DOI: 10.1088/1748-9326/aa7989

Marty, C., Schlogl, S., Bavay, M., & Lehning, M. (2017). How much can we save? Impact of different emission scenarios on future snow cover in the Alps. *Cryosphere*, *11*, 517-529. DOI: 10.5194/tc-11-517-2017

Matteodo, M., Ammann, K., Verrecchia, E.P., & Vittoz, P. (2016). Snowbeds are more affected than other subalpine–alpine plant communities by climate change in the Swiss Alps. *Ecology and Evolution*, *6*, 6969-6982. DOI: 10.1002/ece3.2354

Mihai, B., Nistor, C., Toma, L., & Săvulescu, I. (2016). High resolution landscape change analysis with CORONA KH-4B imagery. A case study from Iron Gates Reservoir Area. *Procedia Environmental Sciences*, *32*, 200-210. DOI: 10.1016/j.proenv.2016.03.025

Molotch, N.P., & Margulis, S.A. (2008). Estimating the distribution of snow water equivalent using remotely sensed snow cover data and a spatially distributed snowmelt model: A multi–resolution, multi–sensor comparison. *Advances in Water Resources*, *31*, 1503-1514. DOI: 10.1016/j.advwatres.2008.07.017

Myers-Smith, I.H., Elmendorf, S.C., Beck, P.S., Wilmking, M., Hallinger, M., Blok, D., Tape, K.D., Rayback, S.A., Macias-Fauria, M., & Forbes, B.C. (2015). Climate sensitivity of shrub growth across the tundra biome. *Nature Climate Change*, *5*, 887-891. DOI: 10.1038/nclimate2697

Myers-Smith, I.H., Forbes, B.C., Wilmking, M., Hallinger, M., Lantz, T., Blok, D., Tape, K.D., Macias-Fauria, M., Sass-Klaassen, U., & Lévesque, E. (2011). Shrub expansion in tundra ecosystems: dynamics, impacts and research priorities. *Environmental Research Letters*, *6*, 045509. DOI: http: //dx.doi.org/10.1088/1748-9326/6/4/045509

Myers-Smith, I.H., Kerby, J.T., Phoenix, G.K., Bjerke, J.W., Epstein, H.E., Assmann, J.J., John, C., Andreu-Hayles, L., Angers-Blondin, S., & Beck, P.S. (2020). Complexity revealed in the greening of the Arctic. *Nature Climate Change*, *10*, 106-117. DOI: 10.1038/s41558-019-0688-1

Niittynen, P., & Luoto, M. (2018). The importance of snow in species distribution models of arctic vegetation. *Ecography*, *41*, 1024-1037. DOI: 10.1111/ecog.03348

Niittynen, P., Heikkinen, R. K., & Luoto, M. (2018). Snow cover is a neglected driver of arctic biodiversity loss. *Nature Climate Change*, *8*, 997-1001. DOI: https://doi.org/10.1038/s41558-018-0311-x

Peterson, E. (2005). Estimating cover of an invasive grass (*Bromus tectorum*) using tobit regression and phenology derived from two dates of Landsat ETM+ data. *International Journal of Remote Sensing*, *26*, 2491-2507. DOI: 10.1080/01431160500127815

Pörtner, H., Roberts, D., Masson-Delmotte, V., Zhai, P., Tignor, M., Poloczanska, E., Mintenbeck, K., Alegría, A., Nicolai, M., & Okem, A. (2019). IPCC special report on the ocean and cryosphere in a changing climate (SROCC). In: Cambridge University Press

Randin, C.F., Vuissoz, G., Liston, G.E., Vittoz, P., & Guisan, A. (2009). Introduction of snow and geomorphic disturbance variables into predictive models of alpine plant distribution in the Western Swiss Alps. *Arctic, Antarctic, and Alpine Research*, *41*, 347-361. DOI: 10.1657/1938-4246-41.3.347

Räsänen, A., & Virtanen, T. (2019). Data and resolution requirements in mapping vegetation in spatially heterogeneous landscapes. *Remote Sensing of Environment*, *230*, 111207. DOI: 10.1016/j.rse.2019.05.026

RE Hernάndez-Lambrao, Carbonell, R. , & JN Sάnchez-Agudo. (2020). Making the most of scarce data: mapping distribution range and variation in population abundance of a threatened narrow-range endemic plant. *Journal for Nature Conservation, 57*, 125889. DOI: https://doi.org/10.1016/j.jnc.2020.125889

Riley, S.J., DeGloria, S.D., & Elliot, R. (1999). A terrain ruggedness index that quantifies topographic heterogeneity. *Intermountain Journal of Sciences 5*: 1–4.

Rixen, C., Schwoerer, C., & Wipf, S. (2010). Winter climate change at different temporal scales in *Vaccinium myrtillus*, an Arctic and alpine dwarf shrub. *Polar Research*, *29*, 85-94. DOI: 10.1111/j.1751-8369.2010.00155.x

Rixen, C., & Wipf, S. (2017). Non-equilibrium in Alpine Plant Assemblages: Shifts in Europe's Summit Floras. High mountain conservation in a changing world (pp. 285-303): Springer

Rosenthal, W., & Dozier, J. (1996). Automated mapping of montane snow cover at subpixel resolution from the Landsat Thematic Mapper. *Water Resources Research*, *32*, 115-130. DOI: 10.1029/95WR02718

Rumpf, S.B., Hülber, K., Wessely, J., Willner, W., Moser, D., Gattringer, A., Klonner, G., Zimmermann, N.E., & Dullinger, S. (2019). Extinction debts and colonization credits of non-forest plants in the European Alps. *Nature Communications*, *10*, 1-9. DOI: 10.1038/s41467-019-12343-x

Sandvik, S.M., & Odland, A. (2014). Changes in alpine snowbed ‐ wetland vegetation over three decades in northern Norway. *Nordic Journal of Botany*, *32*, 377-384. DOI: 10.1111/j.1756-1051.2013.00249.x

Scharnagl, K., Johnson, D., & Ebert-May, D. (2019). Shrub expansion and alpine plant community change: 40-year record from Niwot Ridge, Colorado. *Plant Ecology & Diversity*, *12*, 407-416. DOI: 10.1080/17550874.2019.1641757

Selkowitz, D.J. (2010). A comparison of multi-spectral, multi-angular, and multi-temporal remote sensing datasets for fractional shrub canopy mapping in Arctic Alaska. *Remote Sensing of Environment*, *114*, 1338-1352. DOI: 10.1016/j.rse.2010.01.012

Shen, J., & Tan, F. (2020). Effects of DEM resolution and resampling technique on building treatment for urban inundation modeling: a case study for the 2016 flooding of the HUST campus in Wuhan. *Natural Hazards*, *104(1)*, 927-957. DOI: 10.1007/s11069-020-04198-z

Small, C. (2003). High spatial resolution spectral mixture analysis of urban reflectance. *Remote sensing of environment*, *88(1-2)*, 170-186. DOI: 10.1016/j.rse.2003.04.008

Smith, M. O., Ustin, S. L., Adams, J. B., & Gillespie, A. R. (1990). Vegetation in deserts: I. A regional measure of abundance from multispectral images. *Remote sensing of Environment*, *31(1)*, 1-26. DOI: 10.1016/0034-4257(90)90074-V

Sturm, M., Holmgren, J., McFadden, J.P., Liston, G.E., Chapin III, F.S., & Racine, C.H. (2001). Snow–shrub interactions in Arctic tundra: a hypothesis with climatic implications. *Journal of Climate*, *14*, 336-344. DOI: 10.1175/1520-0442(2001)0142.0.CO;2

Suess, S., van der Linden, S., Okujeni, A., Griffiths, P., Leitao, P. J., Schwieder, M., & Hostert, P. (2018). Characterizing 32 years of shrub cover dynamics in southern Portugal using annual Landsat composites and machine learning regression modeling. *Remote Sensing of Environment*, *219*, 353-364. DOI: 10.1016/j.rse.2018.10.004

Tape, K., Sturm, M., & Racine, C. (2006). The evidence for shrub expansion in Northern Alaska and the Pan‐Arctic. *Global Change Biology*, *12*, 686-702. DOI: 10.1111/j.1365-2486.2006.01128.x

Teillet, P., Guindon, B., & Goodenough, D. (1982). On the slope-aspect correction of multispectral scanner data. *Canadian Journal of Remote Sensing*, *8*, 84-106. DOI: 10.1080/07038992.1982.10855028

Thuiller, W., Lafourcade, B., Engler, R., & Araújo, M. B. (2009). BIOMOD–a platform for ensemble forecasting of species distributions. *Ecography*, *32(3)*, 369-373. DOI: 10.1111/j.1600-0587.2008.05742.x

van Lier, O.R., Fournier, R.A., Bradley, R.L., & Thiffault, N. (2009). A multi-resolution satellite imagery approach for large area mapping of ericaceous shrubs in Northern Quebec, Canada. *International Journal of Applied Earth Observation and Geoinformation*, *11*, 334-343. DOI: 10.1016/j.jag.2009.05.003

Vowles, T., & Björk, R.G. (2019). Implications of evergreen shrub expansion in the Arctic. *Journal of Ecology*, *107*, 650-655. DOI: 10.1111/1365-2745.13081

Vuorinen, K.E., Oksanen, L., Oksanen, T., Pyykönen, A., Olofsson, J., & Virtanen, R. (2017). Open tundra persist, but arctic features decline—Vegetation changes in the warming Fennoscandian tundra. *Global Change Biology*, *23*, 3794-3807. DOI: 10.1111/gcb.13710

Wada, N., & Nakai, Y., (2004). Germinability of seeds in a glacial relict *Dryas octopetala* var. *asiatica*: comparison with a snowbed alpine plant *Sieversia pentapetala* in a middle-latitude mountain area of central japan. *Far Eastern Studies Fes*, *3*, 57-72.

Walker, D., Billings, W., & De Molenaar, J. (2001). Snow-vegetation interactions in tundra environments. In (pp. 266-324): Cambridge University Press Cambridge

Wan, Y.-f., Gao, Q.-z., Li, Y., Qin, X.-b., Ganjurjav, Zhang, W.-n., Ma, X., & Liu, S. (2014). Change of snow cover and its impact on alpine vegetation in the source regions of large rivers on the Qinghai-Tibetan Plateau, China. *Arctic, Antarctic, and Alpine Research*, *46*, 632-644. DOI: 10.1657/1938-4246-46.3.632

Wang, S., Wang, X., Chen, G., Yang, Q., Wang, B., Ma, Y., & Shen, M. (2017). Complex responses of spring alpine vegetation phenology to snow cover dynamics over the Tibetan Plateau, China. *Science of the Total Environment*, *593*, 449-461. DOI: 10.1016/j.scitotenv.2017.03.187

Weisberg, P.J., Dilts, T.E., Baughman, O.W., Meyer, S.E., Leger, E.A., Van Gunst, K.J., & Cleeves, L. (2017). Development of remote sensing indicators for mapping episodic die-off of an invasive annual grass (*Bromus tectorum*) from the Landsat archive. *Ecological Indicators*, *79*, 173-181. DOI: 10.1016/j.ecolind.2017.04.024

Wheeler, J., Hoch, G., Cortés, A.J., Sedlacek, J., Wipf, S., & Rixen, C. (2014). Increased spring freezing vulnerability for alpine shrubs under early snowmelt. *Oecologia*, *175*, 219-229. DOI:

10.1007/s00442-013-2872-8

Willmott, C.J. (1982). Some comments on the evaluation of model performance. *Bulletin of the American Meteorological Society*, *63*, 1309-1313. DOI: 10.1175/1520-0477(1982)063<1309:SCOTEO>2.0.CO;2

Wilson, S.D., & Nilsson, C. (2009). Arctic alpine vegetation change over 20 years. *Global Change Biology*, *15*, 1676-1684. DOI: 10.1111/j.1365-2486.2009.01896.x

Winkler, D.E., Butz, R.J., Germino, M.J., Reinhardt, K., & Kueppers, L.M. (2018). Snowmelt timing regulates community composition, phenology, and physiological performance of alpine plants. *Frontiers in Plant Science*, *9*, 1140. DOI: 10.3389/fpls.2018.01140

Wipf, S. (2010). Phenology, growth, and fecundity of eight subarctic tundra species in response to snowmelt manipulations. *Plant Ecology*, *207*, 53-66. DOI: 10.1007/s11258-009-9653-9

Wipf, S., & Rixen, C. (2010). A review of snow manipulation experiments in Arctic and alpine tundra ecosystems. *Polar Research*, *29*, 95-109. DOI: 10.3402/polar.v29i1.6054

Wipf, S., Rixen, C., & Mulder, C.P. (2006). Advanced snowmelt causes shift towards positive neighbour interactions in a subarctic tundra community. *Global Change Biology*, *12*, 1496-1506. DOI: 10.1111/j.1365-2486.2006.01185.x

Wipf, S., Stoeckli, V., & Bebi, P. (2009). Winter climate change in alpine tundra: plant responses to changes in snow depth and snowmelt timing. *Climatic Change*, *94*, 105-121. DOI: 10.1007/s10584-009-9546-x

Xiao, J., & Moody, A. (2005). A comparison of methods for estimating fractional green vegetation cover within a desert-to-upland transition zone in central New Mexico, USA. *Remote sensing of environment*, *98(2-3)*, 237-250. DOI: 10.1016/j.rse.2005.07.011

Yu, J., Chen, D., Lin, Y., & Ye, S. (2017). Comparison of linear and nonlinear spectral unmixing approaches: a case study with multispectral TM imagery. *International Journal of Remote Sensing*, *38(3)*, 773-795. DOI: 10.1080/01431161.2016.1271475

Zhang, G., Liu, Q., Xu, Q., & Liu, Y. (2010). Soil nitrogen mineralization and primary productivity in *Rhododendron aureum* community of snowpacks in alpine tundra of Changbai Mountain. *Chinese Journal of Applied Ecology*, *21*, 2187-2193. DOI: 10.3724/SP.J.1142.2010.40486 (In Chinese)

Zhu, Z., Wang, S., & Woodcock, C. E. (2015). Improvement and expansion of the Fmask algorithm: Cloud, cloud shadow, and snow detection for Landsats 4-7, 8, and Sentinel 2 images. *Remote Sensing of Environment*, *159*, 269-277. DOI: 10.1016/j.rse.2014.12.014

Zong, S., Jin, Y., Xu, J., Wu, Z., He, H., Du, H., & Wang, L. (2016). Nitrogen deposition but not climate warming promotes *Deyeuxia angustifolia* encroachment in alpine tundra of the Changbai Mountains, Northeast China. *Science of the Total Environment*, *544*, 85-93. DOI: 10.1016/j.scitotenv.2015.11.144

Zong, S., Wu, Z., Xu, J., Li, M., Gao, X., He, H., Du, H., & Wang, L. (2014). Current and potential tree locations in tree line ecotone of Changbai mountains, Northeast China: the controlling effects of topography. *Plos One*, *9*, e106114. DOI: https://doi.org/10.1371/journal.pone.0106114

Zuur, A.F., Ieno, E.N., & Elphick, C.S. (2010). A protocol for data exploration to avoid common statistical problems. *Methods in Ecology and Evolution*, *1*, 3-14. DOI: 10.1111/j.2041-210X.2009.00001.x

List of Figure Captions

Figure 1. Upper Left: location of Changbai Mountains in Northeast China. Lower left: The alpine tundra in the study region, extending from 1850 to the summit at 2749 m (bottom). The red star represents the location of the climate station at the summit of the Changbai Mountains. The yellow line represents the international boundary between China and North Korea. Plots for ground truthing are indicated as green points. Right: field photos: (A) early autumn, 1 September 2017; (B) spring, 13 June 2017; and (C) early spring, 22 May 2015, showing the study site landscape at high (above 2300 m), mid (2000-2300 m), and low elevations (1850-2000 m), respectively. Plant communities with green color in the field photos indicate *R. aureum* communities. Panel (B) shows *R. aureum* in white bloom. Plant communities with yellow and gray color are deciduous shrubs and sedge communities in (A) and herb communities in (B) and (C).

Figure 2. Schematic workflow that summarizes data preparation and processing steps, including the estimation of *Rhododendron aureum* fraction cover time series based on NDVI from Landsat images and high resolution images and field survey data (left), extraction of environmental data, most importantly the assessment of snow cover trends and snowmelt date based on various satellite datasets (right), and integration of both into two models for *R. aureum* (bottom). *RA* = *R. aureum*. HR refers to high

resolution. PPI is the pixel purity index while MNF stands for minimum noise fraction transformation with ENVI. LST refers to land surface temperature derived from Landsat images. ① NDVI calibration includes orthorectification, atmospheric and radiometric calibrations; ② Harmonizations of multi-source images with ENVI; ③ C correction method for terrain correction.

Figure 3. True color RGB image of Sentinel-2 (middle and right) and field photos (left) taken in the alpine tundra of the Changbai Mountains at peak (a) and end (b) of the growing season. Green color at the end of the growing season represents the evergreen shrub, *R. aureum*; the white circle marks a distinctive rock for reference.

Figure 4. Correspondence between plant cover of *R. aureum* (green color) and herbs (brown color, as shown in Figure 1 C) in a 1 m^2 field survey plot and the NDVI value of a GF-2 high-resolution satellite image (23 September 2017, pixel size = 1 m). Number of plots = 165. The lines represent the results from generalized linear regressions (the *glm* function with 'logit' link from the 'MASS' package in R 2020).The grey zone indicates the 0.95 confidence interval.

Figure 5. Scatterplot comparing Landsat shrub fraction to high resolution (HR) shrub abundance (the proportion of *R. aureum* footprints in each Landsat pixel). The black line represents the linear regression line fitting data that starts from the tipping point (0.27) onward.

Figure 6. Pixel-level trends in snow cover (i.e., the coefficient of the ‘year’-term in the generalized linear model) during the snowmelt period (1 April to 15 June) along elevation gradients in the alpine tundra of the Changbai Mountains from 1965 to 2019.

Figure 7. *R. aureum* fraction cover dynamics for increasing fraction cover (top four panels) and decreasing cover (bottom four) pixels for the years 1988, 1992, 2001, 2004, 2009, 2013, and 2019.

Figure 8. Change in fraction cover of *Rhododendron aureum* along elevation gradient between 1988 and 2019. Linear unmixing model was applied to extract fractional cover of *R. aureum* in 1988 and 2019.

Figure 9. The snowmelt regime preference of the evergreen shrub, *Rhododendron aureum*. The response curve as a function of snowmelt day (DOY = day of year) is based on a generalized linear model. The vertical lines on the x-axis in a) indicate distribution density of *R. aureum*. The variable importance scores are mean values from all four species distribution modelling methods. LST indicates land surface temperature derived from Landsat imagery. TWI indicates topographical wetness index.

Figure 10. The projected distributions of *Rhododendron aureum* (represented in green) under current (a) and future snowmelt scenarios (b) based on a species distribution model. The number of pixels (c) and distribution frequencies along the elevation gradient (d) of *R. aureum* as predicted under scenarios for the current snowmelt regime and a future regime. The dashed lines indicate the elevation optimum in each scenario.